



HAL
open science

Influence of periodically fluctuating material parameters on the stability of explicit high-order spectral element methods

Ruben Sevilla, Régis Cottereau

► **To cite this version:**

Ruben Sevilla, Régis Cottereau. Influence of periodically fluctuating material parameters on the stability of explicit high-order spectral element methods. *Journal of Computational Physics*, 2018, 373, pp.304 - 323. 10.1016/j.jcp.2018.07.002 . hal-01898567

HAL Id: hal-01898567

<https://hal.science/hal-01898567>

Submitted on 4 Nov 2018

HAL is a multi-disciplinary open access archive for the deposit and dissemination of scientific research documents, whether they are published or not. The documents may come from teaching and research institutions in France or abroad, or from public or private research centers.

L'archive ouverte pluridisciplinaire **HAL**, est destinée au dépôt et à la diffusion de documents scientifiques de niveau recherche, publiés ou non, émanant des établissements d'enseignement et de recherche français ou étrangers, des laboratoires publics ou privés.

Influence of periodically fluctuating material parameters on the stability of explicit high-order spectral element methods

Ruben Sevilla*

Zienkiewicz Centre for Computational Engineering, College of Engineering, Swansea University, Swansea, SA1 8EN, Wales, UK.

Régis Cottreau

MSSMat, CNRS, CentraleSupélec, Université Paris-Saclay, France

Abstract

This paper aims at studying the influence of material heterogeneity on the stability of explicit time marching schemes for the high-order spectral element discretisation of wave propagation problems. A periodic fluctuation of the density and stiffness parameters is considered, where the period is related to the characteristic element size of the mesh. A new stability criterion is derived analytically for quadratic and cubic one-dimensional spectral elements in heterogeneous materials by using a standard Von Neumann analysis. The analysis presented illustrates the effect of material heterogeneity on the stability limit and also reveals the origin of instabilities that are often observed when the stability limit derived for homogeneous materials is adapted by simply changing the velocity of the wave to account for the material heterogeneity. Several extensions of the results derived for quadratic and cubic one-dimensional spectral elements are discussed, including higher order approximations, different periodicity of the material parameters and higher dimensions. Extensive numerical results demonstrate the validity of the new stability limits derived for heterogeneous materials with periodic fluctuation. Finally numerical examples of the

*Corresponding author

Email address: r.sevilla@swansea.ac.uk (Ruben Sevilla)

stability for randomly fluctuating material properties are also presented, discussing the applicability of the theoretical limits derived for material properties with periodic fluctuation.

Keywords: spectral element method, explicit time integration, stability, heterogeneous media, high-order

1. Introduction

Explicit time marching schemes for high-order spectral element discretisations of wave propagation problems are known to be conditionally stable [1]. For a homogeneous one-dimensional problem with constant element size, the stability criterion is given by

$$\alpha = \frac{c\Delta t}{h} \leq \alpha_M, \quad (1)$$

where c is the wave velocity, Δt is the time step, and h is the characteristic element size. The stability limit, α_M , is a scalar that depends upon the polynomial order p and the dimensionality of the problem d . Its value can be derived analytically for homogeneous media [1, 2, 3, 4, 5]. Table 1 summarises the values for polynomial approximations up to order $p = 5$ when the spectral element method is combined with the Leap-Frog time marching scheme. For regular meshes in d dimensions, the value of the stability limit is simply that for one-dimensional problems divided by \sqrt{d} .

Table 1: Approximate value of the stability limit α_M for spectral elements of polynomial order p with the Leap-Frog scheme assuming a regular mesh and constant wave velocity.

$p =$	1	2	3	4	5
1D	1.00	0.40	0.23	0.14	0.10
2D	0.70	0.28	0.16	0.10	0.07
3D	0.57	0.23	0.13	0.08	0.05

10 The results in Table 1 are derived for homogeneous material parameters and
 11 regular meshes. Numerical tests showing the negative influence of the deforma-
 12 tion of the elements on the stability are reported in [1]. Some hints can also be
 13 found about the error induced by the presence of a discontinuity or heterogene-
 14 ity of the material properties [6, 7, 1], but no general stability criteria exists in
 15 that case. A rule of thumb extending Equation (1) is typically applied, in which
 16 (i) the polynomial order is indirectly taken into account by choosing h as the
 17 smallest distance between two interpolation points in an element, (ii) element-
 18 wise maximum, average, or local value of the velocity $c(x)$ is chosen, and (iii) a
 19 heuristic value of the stability criteria α_M is considered. Most authors (see for
 20 instance [8, 9, 10]) choose a stability criterion close to 0.3-0.4, but it can go
 21 as high as 0.6 [11, 12], or as low as 0.07 for non-conforming meshes [13] (with
 22 a discontinuous Galerkin approach). As with any heuristic criterion, the risk
 23 is either to run into unstable cases by considering a high value or to waste
 24 computational resources by employing a low value.

25 This paper aims at describing the influence of material heterogeneity on
 26 the stability of explicit time marching schemes for the high-order spectral el-
 27 ement discretisation of wave propagation problems. A periodic fluctuation of
 28 the density and stiffness parameters is considered, whose period is related to
 29 the characteristic element size h . A classical Von Neumann stability analysis
 30 is performed for quadratic and cubic spectral elements in one dimension. This
 31 analysis not only provides an analytical stability limit but also demonstrates
 32 that a heuristic approach can lead to unstable simulations or to unnecessary ex-
 33 pensive simulations when the stability limit derived for the homogeneous case is
 34 adapted by simply changing the velocity of the wave to account for the material
 35 heterogeneity. It is worth noting that this is true even for relative low orders
 36 of approximation (e.g. $p = 2$). Several extensions of the results derived for
 37 quadratic and cubic one-dimensional spectral elements are discussed, including
 38 higher order approximations, different periodicity of the material parameters
 39 and higher dimensions. A number of numerical examples are presented to show
 40 the validity of the stability limits obtained. These values are also compared with

41 the stability limits that would be derived from the results available in the liter-
 42 ature for homogeneous materials. Finally, the paper presents several numerical
 43 examples to discuss the validity of the stability limits obtained for periodically
 44 fluctuating material properties when applied to problems with randomly fluc-
 45 tuating material properties.

46 2. Problem statement and discretisation

47 2.1. Weak formulation

Let us consider the one-dimensional acoustic wave equation in a heteroge-
 nous medium Ω characterised by a density function $\eta(x)$ and a Lamé parameter
 $\gamma(x)$,

$$\eta(x) \frac{\partial^2 u(x, t)}{\partial t^2} - \frac{\partial}{\partial x} \left(\gamma(x) \frac{\partial u(x, t)}{\partial x} \right) = f(x, t), \quad \text{for } (x, t) \in \Omega \times (0, T], \quad (2)$$

where $u(x, t)$ is a scalar field, $f(x, t)$ denotes a time-dependent external force
 and T denotes the final time. The problem is closed by considering appropriate
 initial and boundary conditions, namely

$$u(x, 0) = u_0(x), \quad \frac{\partial u(x, 0)}{\partial t} = v_0(x), \quad \text{for } x \in \Omega. \quad (3)$$

and

$$u(x, t) = u_d(t), \quad \text{for } x \in \partial\Omega \times (0, T], \quad (4)$$

48 where, to simplify the presentation, only Dirichlet boundary conditions are con-
 49 sidered.

The weak statement equivalent to the strong form (2), is obtained by multi-
 plying Equation (2) by a test function $w(x)$, integrating in the whole domain and
 performing an integration by parts of the term with second order spatial deriva-
 tives. The resulting weak form reads: find $u(x, t) \in \mathcal{W}_t$ such that $u(x, t) = u_d(t)$
 on $\partial\Omega \times [0, T]$ and

$$\int_{\Omega} \eta(x) w(x) \frac{\partial^2 u(x, t)}{\partial t^2} dx + \int_{\Omega} \gamma(x) \frac{\partial w(x)}{\partial x} \frac{\partial u(x, t)}{\partial x} dx = \int_{\Omega} w(x) f(x, t) dx, \quad (5)$$

for all $w(x) \in \mathcal{H}_0^1(\Omega)$, where

$$\mathcal{W}_t = \{u \mid u(\cdot, t) \in \mathcal{H}^1(\Omega), t \in [0, T] \text{ and } u(x, t) = u_d(x, t) \text{ for } (x, t) \in \partial\Omega \times [0, T]\}. \quad (6)$$

50 *2.2. Spatial and temporal discretisation*

The spatial domain is discretised in elements $\Omega_i = [x_i, x_{i+1}]$ and a nodal approximation of the solution is considered within each element using the Gauss-Lobatto-Legendre (GLL) points, denoted by $\{x_i, x_{i,1}, \dots, x_{i,p-1}, x_{i+1}\}$. The first and last GLL points within an element correspond to the vertices, x_i and x_{i+1} , respectively. The approximate solution within an element Ω_i , $u_h^i = u_{h|\Omega_i}$, is given by

$$u_h^i(x, t) = N_i(x)U_i(t) + N_{i+1}(x)U_{i+1}(t) + \sum_{j=1}^{p-1} N_{i,j}(x)U_{i,j}(t), \quad (7)$$

51 where $\{N_i, N_{i,1}, \dots, N_{i,p-1}, N_{i+1}\}$ are Lagrange polynomials of degree p and
 52 $\{U_i, U_{i,1}, \dots, U_{i,p-1}, U_{i+1}\}$ denote the time-dependent values of the solution at
 53 the nodal points.

Introducing the approximation of the solution in the weak formulation of Equation (5) and selecting the space of the weighting functions to be the same as the space of the interpolation functions, leads to the semi-discrete system of ordinary differential equations

$$\mathbf{M} \frac{d^2 \mathbf{U}}{dt^2} + \mathbf{K} \mathbf{U} = \mathbf{F}, \quad (8)$$

where the mass matrix \mathbf{M} , the stiffness matrix \mathbf{K} and the forcing vector \mathbf{F} are given by

$$M_i^j = \int_{\Omega} \eta N_i N_j d\Omega, \quad K_i^j = \int_{\Omega} \gamma \frac{\partial N_i}{\partial x} \frac{\partial N_j}{\partial x} d\Omega, \quad F_i = \int_{\Omega} N_i f d\Omega \quad (9)$$

54 and computed by assembling the elemental contributions.

55 The integrals are computed using a numerical quadrature defined over the
 56 reference element. In a standard finite element method, Gauss-Legendre quadratures
 57 are considered, providing the highest order possible for a given set of inte-
 58 gration points. However, this formulation leads to a dense global mass matrix.

59 In the so-called *spectral element method* (SEM) [14, 15], the quadrature points
60 are selected to be the same as the nodal points (i.e. the GLL distribution),
61 leading to a diagonal global mass matrix.

The main benefit of the SEM is its efficiency when combined with an explicit time marching algorithm. In this work, the classical second-order accurate Leap-Frog scheme is considered. At each time step, the solution is advanced in time according to

$$\mathbf{U}^{n+1} = 2\mathbf{U}^n - \mathbf{U}^{n-1} + \Delta t^2 \mathbf{M}^{-1} (\mathbf{F}^n - \mathbf{K}\mathbf{U}^n), \quad (10)$$

62 where it is worth emphasising that, in the context of the SEM, each time step
63 only involves the solution of a trivial system of equations with diagonal mass
64 matrix.

65 3. Stability analysis for quadratic spectral elements

In this section, the model problem of Equation (2) is considered in $\Omega = \mathbb{R}$ with no external forces and the classical Von Neumann stability analysis is performed for the SEM with quadratic elements. A one-dimensional uniform mesh is considered where the element size is defined as

$$h = x_{i+1} - x_i, \quad \forall i \in \mathbb{Z} \quad (11)$$

and the material properties are considered periodic, with period equal to the element size h , that is

$$\gamma(x) = \gamma(x + rh) \quad \text{and} \quad \eta(x) = \eta(x + rh), \quad \forall x \in \Omega, \quad \forall r \in \mathbb{Z}. \quad (12)$$

66 3.1. Dispersion relations

The SEM produces the following semi-discrete equations

$$M_i^i \frac{d^2 U_i}{dt^2} + (K_{i-1}^i U_{i-1} + K_{i-1,1}^i U_{i-1,1} + K_i^i U_i + K_{i,1}^i U_{i,1} + K_{i+1}^i U_{i+1}) = 0, \quad (13)$$

$$M_{i,1}^{i,1} \frac{d^2 U_{i,1}}{dt^2} + (K_i^{i,1} U_i + K_{i,1}^{i,1} U_{i,1} + K_{i+1}^{i,1} U_{i+1}) = 0, \quad (14)$$

for a vertex and an interior node of a quadratic element respectively where, using the corresponding GLL quadrature points, the terms of the mass and stiffness matrix are given by

$$M_i^i = \frac{h}{3}\eta_i, \quad M_{i,1}^{i,1} = \frac{2h}{3}\eta_{i,1}, \quad K_i^i = \frac{2}{3h}(5\gamma_i + \gamma_{i,1}), \quad K_{i,1}^{i,1} = \frac{16}{3h}\gamma_i, \quad (15)$$

$$K_{i-1,1}^i = K_{i,1}^i = K_i^{i,1} = -\frac{8}{3h}\gamma_i, \quad K_{i-1}^i = K_{i+1}^i = \frac{1}{3h}(3\gamma_i - 2\gamma_{i,1}). \quad (16)$$

Assuming plane wave solutions

$$U_i = \alpha_1 e^{I(ikh - w_h t)} \quad U_{i,1} = \alpha_2 e^{I[(i+1/2)kh - w_h t]}, \quad (17)$$

with $I = \sqrt{-1}$, Equations (13) and (14) lead to the following generalised eigenvalue problem

$$\widehat{\mathbf{K}} \begin{pmatrix} \alpha_1 \\ \alpha_2 \end{pmatrix} = w_h^2 \widehat{\mathbf{M}} \begin{pmatrix} \alpha_1 \\ \alpha_2 \end{pmatrix} \quad (18)$$

where

$$\widehat{\mathbf{K}} = \begin{pmatrix} 2 \cos(kh) K_{i+1}^i + K_i^i & K_{i-1,1}^i e^{-Ikh/2} + K_{i,1}^i e^{Ikh/2} \\ K_{i,1}^i e^{-Ikh/2} + K_{i-1,1}^i e^{Ikh/2} & K_{i,1}^{i,1} \end{pmatrix} \quad (19)$$

and

$$\widehat{\mathbf{M}} = \begin{pmatrix} M_i^i & 0 \\ 0 & M_{i,1}^{i,1} \end{pmatrix}. \quad (20)$$

The characteristic equation of the generalised eigenvalue problem (18) is

$$\left(\frac{hw_h}{c_\star} \right)^4 - 4(6\beta^2 - \delta\omega^2) \left(\frac{hw_h}{c_\star} \right)^2 + 96\beta^2\omega^2 = 0, \quad (21)$$

with

$$c_\star^2 = \frac{\gamma_i + 2\gamma_{i,1}}{\eta_i + 2\eta_{i,1}}, \quad \beta^2 = \frac{1}{c_\star^4} \frac{\gamma_i(\gamma_i + 2\gamma_{i,1})}{3\eta_i\eta_{i,1}}, \quad \delta = \frac{1}{c_\star^2} \frac{3\gamma_i - 2\gamma_{i,1}}{\eta_i}, \quad \omega = \sin(kh/2). \quad (22)$$

67 The parameter c_\star has units of velocity whereas $\beta > 0$, δ and ω are dimensionless.

68 The parameter δ may be positive or negative, depending on the sign of $3\gamma_i - 2\gamma_{i,1}$.

69 The homogeneous case ($\gamma_i = \gamma_{i,1}$ and $\eta_i = \eta_{i,1}$) corresponds to $\beta = \delta = 1$ and

70 $c_\star^2 = \gamma_i/\eta_i = \gamma_{i,1}/\eta_{i,1}$.

71 It is worth mentioning that the velocity c_* corresponds to the approxima-
72 tion of $\sqrt{\int_{\Omega_i} \gamma(x) / \int_{\Omega_i} \eta(x)}$ by using the GLL quadrature with three integration
73 points.

The roots of the characteristic polynomial of Equation (21) are

$$w_{h,1}^2 = 2 \left(\frac{c_*}{h} \right)^2 \left((6\beta^2 - \delta\omega^2) - \sqrt{(6\beta^2 - \delta\omega^2)^2 - 24\beta^2\omega^2} \right), \quad (23)$$

$$w_{h,2}^2 = 2 \left(\frac{c_*}{h} \right)^2 \left((6\beta^2 - \delta\omega^2) + \sqrt{(6\beta^2 - \delta\omega^2)^2 - 24\beta^2\omega^2} \right), \quad (24)$$

74 which reduce to the roots of the homogeneous case considered in [1] when $\beta =$
75 $\delta = 1$.

The Taylor series expansion of the two roots leads to

$$w_{h,1}^2 = c_*^2 k^2 \left[1 + \frac{1 + \delta - 2\beta^2}{24\beta^2} k^2 h^2 + \mathcal{O}(k^4 h^4) \right], \quad (25)$$

$$w_{h,2}^2 = c_*^2 k^2 \left[\frac{24\beta^2}{k^2 h^2} - (1 + \delta) - \frac{1}{24\beta^2} (1 + \delta)(1 - 2\beta^2) k^2 h^2 + \mathcal{O}(k^4 h^4) \right], \quad (26)$$

76 where it can be observed that Equation (25) corresponds to an approximation of
77 the dispersion relation of the wave equation whereas Equation (26) corresponds
78 to a parasitic wave.

79 It is worth noting that the particular case of a medium with $\delta - 2\beta^2 = 1$ in-
80 duces a superconvergent phenomenon as the Taylor expansion of Equation (25)
81 is of order four. Superconvergence has been previously reported for homoge-
82 neous medium [1] but the analysis presented here shows that this behaviour
83 can also be obtained for a heterogeneous medium. However, it is important to
84 note that the objective of the Taylor expansion of the roots is to distinguish the
85 parasitic wave from the physical wave rather than to extract any conclusions
86 about the accuracy of the roots as the element size h tends to zero.

87 3.2. Stability for the Leap-Frog scheme

The dispersion relations for the SEM with a Leap-Frog time integrator are
given by

$$\frac{4}{\Delta t^2} \sin^2 \left(\frac{w_{h,l}^2 \Delta t}{2} \right) = w_{h,l}^2, \quad \text{for } l = 1, 2. \quad (27)$$

The stability of the discrete scheme is controlled by the conditions $w_{h,l}^2 \Delta t^2 \leq 4$ for $l = 1, 2$, that is

$$\sqrt{\max_{l=1,2} \left\{ \sup_{\omega \in [-1,1]} w_{h,l}^2(\omega), 0 \right\}} \leq \frac{2}{\Delta t}. \quad (28)$$

The supremum of the roots is found by studying the zeros of $\partial w_{h,l}^2 / \partial \omega$ for $l = 1, 2$. Firstly, $\partial w_{h,1}^2 / \partial \omega$ only vanishes if $\delta = -1$ or $\omega = 0$. If $\delta = -1$, $w_{h,1}^2 = 4c_\star^2 \omega^2 / h^2$, whose maximum is $4c_\star^2 / h^2$. Otherwise, the supremum is attained for $\omega = 0$ or in the bounds of the interval, namely $\omega = -1$ and $\omega = 1$. Observing that $w_{h,1}^2(-1) = w_{h,1}^2(1) = 2c_\star^2(6\beta^2 - \delta - \sqrt{(6\beta^2 - \delta)^2 - 24\beta^2}) / h^2$, leads to (the second value includes the maximum obtained for the special case when $\delta = -1$)

$$\sup_{\omega \in [-1,1]} w_{h,1}^2(\omega) = 2 \frac{c_\star^2}{h^2} \max \left\{ 0, 6\beta^2 - \delta - \sqrt{(6\beta^2 - \delta)^2 - 24\beta^2} \right\}. \quad (29)$$

Secondly, $\partial w_{h,2}^2 / \partial \omega$ only vanishes when $\delta = -1$ or $\omega = 0$. If $\delta = -1$, the roots takes a constant value $w_{h,2}^2 = 24(\beta c_\star / h)^2$. Otherwise, observing that $w_{h,2}^2(0) = 24(\beta c_\star / h)^2$ and that at the bounds of the interval $w_{h,2}^2(-1) = w_{h,2}^2(1) = 2c_\star^2(6\beta^2 - \delta + \sqrt{(6\beta^2 - \delta)^2 - 24\beta^2}) / h^2$, leads to

$$\sup_{\omega \in [-1,1]} w_{h,2}^2(\omega) = 2 \frac{c_\star^2}{h^2} \max \left\{ 12\beta^2, 6\beta^2 - \delta + \sqrt{(6\beta^2 - \delta)^2 - 24\beta^2} \right\}. \quad (30)$$

The stability condition is therefore given by

$$\alpha = \frac{c_\star \Delta t}{h} \leq \alpha_M, \quad (31)$$

with

$$\alpha_M := \min \left\{ \frac{\sqrt{6}}{6\beta}, \sqrt{\frac{2}{6\beta^2 - \delta + \sqrt{(6\beta^2 - \delta)^2 - 24\beta^2}}} \right\}. \quad (32)$$

88 It can be observed that the well known homogeneous stability condition $\alpha_M =$
89 $1/\sqrt{6} \approx 0.40$ (see Table 1) is recovered when $\beta = \delta = 1$.

90 3.3. Discussion

The positivity of the polynomial function $P(\beta, \delta) = (6\beta^2 - \delta\omega^2)^2 - 24\beta^2\omega^2$ is discussed next as the square root of this function appears in the stability

constant of Equation (32). It is worth noting that the parameters β and δ can be expressed as a function of the ratios $Q_\gamma = \gamma_{i,1}/\gamma_i$ and $Q_\eta = \eta_{i,1}/\eta_i$ and the velocity c_\star can be expressed as a function of Q_γ , Q_η and the ratio $c_i^2 = \gamma_i/\eta_i$ as

$$\beta^2 = \frac{(1 + 2Q_\eta)^2}{3Q_\eta(1 + 2Q_\gamma)}, \quad \delta = (3 - 2Q_\gamma)\frac{1 + 2Q_\eta}{1 + 2Q_\gamma}, \quad c_\star^2 = c_i^2\frac{1 + 2Q_\gamma}{1 + 2Q_\eta}. \quad (33)$$

Rewriting the polynomial as a function of the ratios of the material properties leads to

$$\frac{Q_\eta^2(1 + 2Q_\gamma)^2}{(1 + 2Q_\eta)^2}P(Q_\gamma, Q_\eta) = (2(1 + 2Q_\eta) - Q_\eta\omega^2(3 - 2Q_\gamma))^2 - 8Q_\eta\omega^2(1 + 2Q_\gamma), \quad (34)$$

and by considering the right-hand side function as a polynomial in Q_γ with positive leading term, its minimum is attained at $Q_\gamma = (2 - 4Q_\eta + 3Q_\eta\omega^2)/(2Q_\eta\omega^2)$. After simplification, the minimum is obtained as

$$\min_{Q_\gamma} \frac{Q_\eta^2(1 + 2Q_\gamma)^2}{(1 + 2Q_\eta)^2}P(Q_\gamma, Q_\eta) = 32Q_\eta(1 - \omega^2). \quad (35)$$

91 As $\omega^2 \in [0, 1]$, the minimum is always positive and it is attained for $\omega^2 = 1$.
 92 Therefore, it is concluded that $P(\beta, \delta) \geq 0$ for all Q_γ and Q_η .

93 Finally, as $6\beta^2 - \delta$ is proportional to $2 + Q_\eta + 6Q_\eta Q_\gamma$ it is clear that $6\beta^2 -$
 94 $\delta + \sqrt{P(\beta, \delta)} \geq 0$, so the stability constant α_M of Equation (32) is always a real
 95 number.

The analysis presented in the previous section not only shows the stability condition for the periodic heterogeneous media considered. More importantly, it explains why the stability limit derived from the homogeneous case can lead to either inefficient simulations or to instabilities if applied to a problem with heterogeneous material properties. In the absence of theoretical results for heterogeneous media, a possible choice for the time step would be to consider the value of α_M of the homogeneous case and the maximum value of the nodal wave velocities [16, 17], that is

$$\Delta t = \frac{h}{\max_i\{c_i\}\sqrt{6}}. \quad (36)$$

96 However, contrary to the homogeneous case, in the heterogeneous case the
 97 supreme of $w_{h,2}$ is not always attained at $\omega = 0$. To illustrate the effect of

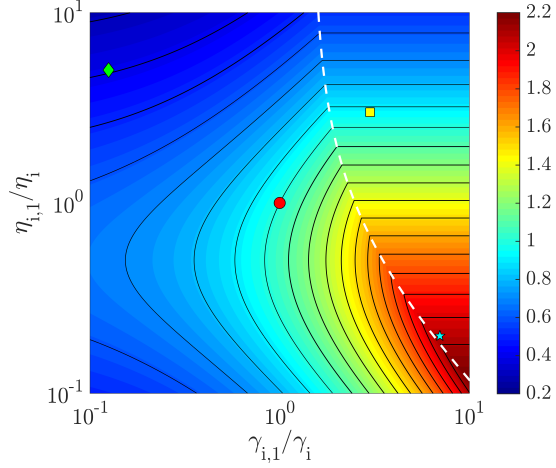


Figure 1: Ratio between the value of α_M for the heterogeneous and homogeneous cases for different values of the ratios $Q_\gamma = \gamma_{i,1}/\gamma_i$ and $Q_\eta = \eta_{i,1}/\eta_i$. The red dot indicates the homogeneous case and the white discontinuous line represents the change of definition of α_M given by maximum in Equation (31). The other symbols correspond to the numerical experiments presented in Section 3.4.

98 the heterogeneity in the stability limit, Figure 1 shows the ratio between the
 99 value of α_M for the heterogeneous and homogeneous cases for different values of
 100 the ratios Q_γ and Q_η . When the ratio between the value of α_M for the heteroge-
 101 neous and homogeneous cases is lower than one, the expression of Equation (36)
 102 will lead to unstable results. In contrast, when the ratio is higher than one, us-
 103 ing Equation (36) will result in an unnecessary increased computational cost.
 104 It is important to emphasise that depending upon the fluctuation of the mate-
 105 rial parameters, the value of α_M for the heterogeneous and homogeneous cases
 106 can differ significantly. For a fluctuation up to one order of magnitude in the
 107 values of γ and η , the ratio between the value of α_M for the heterogeneous
 108 and homogeneous cases varies between 0.2 and 2.2 as shown in Figure 1. The
 109 discontinuous line in Figure 1 denotes the change of definition in the maximum
 110 appearing in the denominator of Equation (32), which corresponds to $\delta = -1$
 111 or, equivalently, to $Q_\eta(2Q_\gamma - 3) = 2$.

112 Interestingly, this figure can also be used as a guide for generating the com-

113 putational mesh. Indeed, the strong asymmetry between the values of the pa-
 114 rameters in the middle of the elements and at the vertices means that it is
 115 preferable to mesh the domain with elements such that the low values of the
 116 parameter $\eta(x)$ and the high values of the parameter $\gamma(x)$ fall in the middle
 117 of the elements. In particular, for periodic materials and meshes, it is always
 118 possible to translate the mesh, and therefore to move around in Figure 1 so as
 119 to optimise the time step. Note that such a translation would also impact the
 120 accuracy, which is not considered here.

121 3.4. Numerical examples

Three numerical examples are presented to validate the stability condition
 derived in this Section and to illustrate that using a condition derived for the
 homogeneous case can lead to either unstable results or inefficient computations.
 The domain $\Omega = [0, 1]$ is considered and the material parameters are defined as

$$\gamma(x) = \gamma_i + (\gamma_{i,1} - \gamma_i) \sin^2(\pi x/h), \quad \eta(x) = \eta_i + (\eta_{i,1} - \eta_i) \sin^2(\pi x/h), \quad (37)$$

122 where both functions are defined in terms of the values of the material parameter
 123 at the vertices (γ_i and η_i) and at the interior nodes ($\gamma_{i,1}$ and $\eta_{i,1}$).

The analytical solution is given by

$$u(x, t) = \cos(2\pi t) \sin(2\pi x) \quad (38)$$

124 and the initial, boundary conditions and source term are derived from the exact
 125 solution as usually done in the method of manufactured solutions. In all the
 126 examples, the solution is advanced in time up to a final time $T = 10$ and the
 127 relative error in the $\mathcal{L}^2(\Omega)$ norm is measured. It is worth emphasising that
 128 the objective of the numerical examples is not to evaluate the accuracy of the
 129 numerical scheme but the accuracy of the stability limit derived for quadratic
 130 spectral elements with a periodic fluctuation of the material properties.

131 The first example considers $\gamma_i = 1$, $\gamma_{i,1} = 3$, $\eta_i = 1$ and $\eta_{i,1} = 3$. The
 132 stability condition given by Equation (32) is $\alpha_M = 1/\sqrt{7} \approx 0.37796$. Figure 2
 133 (a) shows the relative error in the $\mathcal{L}^2(\Omega)$ norm as a function of the value of α

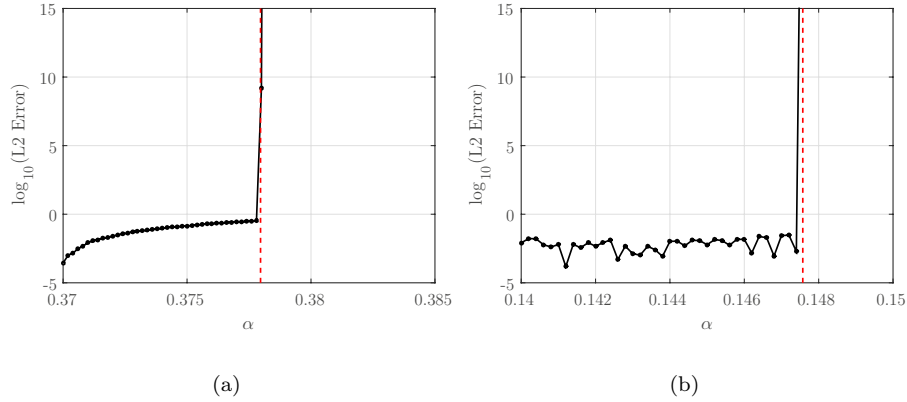


Figure 2: Relative error in the $\mathcal{L}^2(\Omega)$ norm as a function of $\alpha = c_* \Delta t / h$ for (a) $Q_\gamma = 3, Q_\eta = 3$ and (b) $Q_\gamma = 7, Q_\eta = 1/5$. The discontinuous line represents the stability limit corresponding to α_M .

134 considered to define the time step Δt for a uniform mesh with $h = 0.01$. It
 135 can be clearly observed that when the time step is defined by using a value of
 136 $\alpha \leq \alpha_M$ stability is guaranteed, whereas a value of $\alpha > \alpha_M$ leads to unstable
 137 results. More precisely, a value of $\alpha = 0.378$ (i.e, $\Delta t \approx 3.78 \times 10^{-3}$) leads to an
 138 instability, with a final error of 6.1×10^7 whereas a value of $\alpha = 0.37795$ (i.e,
 139 $\Delta t \approx 3.7795 \times 10^{-3}$) leads to stable results, with a final error of 3.77×10^{-4} .
 140 In this example, if the time step is computed using the results derived from the
 141 homogeneous case, as detailed in Equation (36), the result is $\Delta t \approx 4.08 \times 10^{-3}$,
 142 clearly leading to unstable results.

143 The next example considers a higher fluctuation in the material properties,
 144 namely $\gamma_i = 1, \eta_i = 5, \gamma_{i,1} = 7$ and $\eta_{i,1} = 1$. The stability condition given by
 145 Equation (32) is $\alpha_M = 7\sqrt{10}/150 \approx 0.14757$. Figure 2 (b) shows the relative
 146 error in the $\mathcal{L}^2(\Omega)$ norm as a function of the value of α considered to define the
 147 time step Δt for a uniform mesh with $h = 0.01$. As in the previous example, it
 148 can be clearly observed that the stability derived in this section holds.

149 The previous examples considered material parameters such that the min-
 150 imum in Equation (32) is achieved by the first term, i.e. $\alpha_M = 1/(\beta\sqrt{6})$.
 151 The last example considers $\gamma_i = 8, \eta_i = 1, \gamma_{i,1} = 5$ and $\eta_{i,1} = 1$. The pa-

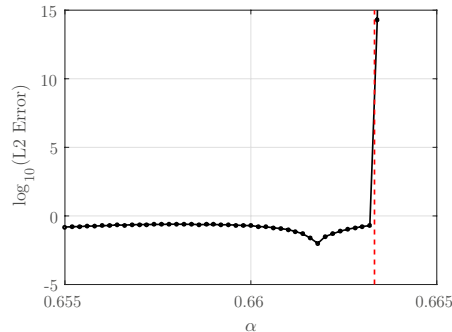


Figure 3: Relative error in the $\mathcal{L}^2(\Omega)$ norm as a function of $\alpha = c_x \Delta t / h$ for $\gamma_i = 8$, $\eta_i = 1$, $\gamma_{i,1} = 5$ and $\eta_{i,1} = 1$. The discontinuous line represents the stability limit corresponding to α_M .

152 parameters have been selected to ensure that the minimum in Equation (32) is
 153 achieved by the second term in Equation (32). The value of the stability limit is
 154 $\alpha_M = \sqrt{11}/5 \approx 0.66332$. As in previous examples, Figure 3 shows the relative
 155 error in the $\mathcal{L}^2(\Omega)$ norm as a function of the value of α considered to define the
 156 time step Δt for a uniform mesh with $h = 0.01$. The results demonstrate the
 157 validity of the stability limit derived in this section. As in the first example,
 158 if the value of the stability limit given by the homogeneous case is considered
 159 unstable results are obtained.

160 4. Stability analysis for cubic spectral elements

161 This Section presents the classical Von Neumann stability analysis for the
 162 SEM with cubic elements for the model problem of Equation (2). Analogously
 163 to the quadratic case, a one-dimensional uniform mesh is considered and the
 164 material properties are assumed periodic, with period equal to the element size.

165 *4.1. Dispersion relations*

Following the procedure presented in Section 3.1, the characteristic equation of the generalised eigenvalue problem for cubic spectral elements is

$$\left(\frac{hw_h}{c_\star}\right)^6 - 2(2\delta_1\omega^2 + 45A_1) \left(\frac{hw_h}{c_\star}\right)^4 + 120(15\beta^2 - 2\delta_2\omega^2) \left(\frac{hw_h}{c_\star}\right)^2 - 7200\beta^2\omega^2 = 0, \quad (39)$$

with

$$c_\star^2 = \frac{36\gamma_i(\gamma_i\gamma_{i,1} + 2\gamma_{i,1}\gamma_{i,2} + \gamma_{i,2}\gamma_i)}{(5\gamma_i^2 + 3\gamma_i\gamma_{i,1} + \gamma_{i,1}\gamma_{i,2} + 3\gamma_{i,2}\gamma_i)(2\eta_i + 5\eta_{i,1} + 5\eta_{i,2})}, \quad (40)$$

$$\beta^2 = \frac{1}{4c_\star^6} \frac{\gamma_i(\gamma_i\gamma_{i,1} + 2\gamma_{i,1}\gamma_{i,2} + \gamma_{i,2}\gamma_i)}{\eta_i\eta_{i,1}\eta_{i,2}}, \quad (41)$$

$$A_1 = \frac{1}{18c_\star^2} \left(\frac{3\gamma_i + \gamma_{i,1}}{\eta_{i,2}} + \frac{3\gamma_i + \gamma_{i,2}}{\eta_{i,1}} + \frac{5}{2} \frac{2\gamma_i + \gamma_{i,1} + \gamma_{i,2}}{\eta_i} \right), \quad (42)$$

$$\delta_1 = \frac{1}{c_\star^2} \frac{12\gamma_i - 5\gamma_{i,1} - 5\gamma_{i,2}}{2\eta_i}, \quad (43)$$

$$\delta_2 = 30 \frac{(\eta_{i,1} + \eta_{i,2})\beta^2}{(2\eta_i + 5\eta_{i,1} + 5\eta_{i,2})} - \frac{1}{4c_\star^4} c_i^2 \left(\frac{\gamma_i + 7\gamma_{i,1}}{\eta_{i,2}} + \frac{\gamma_i + 7\gamma_{i,2}}{\eta_{i,1}} \right). \quad (44)$$

166 The parameter c_\star has units of velocity while $\beta > 0$, $A_1 > 0$, δ_1 , δ_2 and ω are
 167 dimensionless. The parameters δ_1 and δ_2 may be positive or negative. The
 168 homogeneous case ($\gamma_i = \gamma_{i,1} = \gamma_{i,2}$ and $\eta_i = \eta_{i,1} = \eta_{i,2}$) corresponds to $\beta =$
 169 $A_1 = \delta_1 = \delta_2 = 1$ and $c_\star^2 = \gamma_i/\eta_i = \gamma_{i,1}/\eta_{i,1} = \gamma_{i,2}/\eta_{i,2}$.

The roots of the characteristic polynomial of Equation (39) are

$$w_{h,1}^2 = \frac{c_\star^2}{h^2} \left[\sigma_1(\omega) + \sigma_3(\omega) + \frac{\sigma_2(\omega)}{\sigma_3(\omega)} \right], \quad (45)$$

$$w_{h,2}^2 = \frac{c_\star^2}{h^2} \left[\sigma_1(\omega) - \frac{1}{2} \left(\sigma_3(\omega) + \frac{\sigma_2(\omega)}{\sigma_3(\omega)} \right) + \frac{\sqrt{3}}{2} \left(\sigma_3(\omega) - \frac{\sigma_2(\omega)}{\sigma_3(\omega)} \right) I \right], \quad (46)$$

$$w_{h,3}^2 = \frac{c_\star^2}{h^2} \left[\sigma_1(\omega) - \frac{1}{2} \left(\sigma_3(\omega) + \frac{\sigma_2(\omega)}{\sigma_3(\omega)} \right) - \frac{\sqrt{3}}{2} \left(\sigma_3(\omega) - \frac{\sigma_2(\omega)}{\sigma_3(\omega)} \right) I \right], \quad (47)$$

where

$$\sigma_1(\omega) = \frac{2}{3}(2\delta_1\omega^2 + 45A_1), \quad \sigma_2(\omega) = \sigma_1^2(\omega) - 40(15\beta^2 - 2\delta_2\omega^2), \quad (48)$$

$$\sigma_3(\omega) = \left(\sqrt{\sigma^2(\omega) - \sigma_2^3(\omega)} + \sigma(\omega) \right)^{1/3}, \quad (49)$$

$$\sigma(\omega) = \frac{\sigma_1(\omega)}{2} (3\sigma_2(\omega) - \sigma_1^2(\omega)) + 3600\beta^2\omega^2. \quad (50)$$

170 As expected, the roots obtained here reduce to the homogeneous case con-
171 sidered in [1] when $\beta = A_1 = \delta_1 = \delta_2 = 1$.

The Taylor series expansions of σ_1 , $\sigma_3 + \sigma_2/\sigma_3$ and $\sigma_3 - \sigma_2/\sigma_3$ up to second order are given by

$$\sigma_1 = 30A_1 + \mathcal{O}(k^2h^2), \quad (51)$$

$$\sigma_3 + \sigma_2/\sigma_3 = 3^{1/3}10\vartheta^{1/3} + 3^{2/3}10(3A_1^2 - 2\beta^2)\vartheta^{-1/3} + \mathcal{O}(k^2h^2), \quad (52)$$

$$\sigma_3 - \sigma_2/\sigma_3 = 3^{1/3}10\vartheta^{1/3} - 3^{2/3}10(3A_1^2 - 2\beta^2)\vartheta^{-1/3} + \mathcal{O}(k^2h^2), \quad (53)$$

172 where $\vartheta = 9A_1(A_1^2 - \beta^2) + \sqrt{3(9A_1^2 - 8\beta^2)}I$ and it is worth noting that ϑ is
173 complex because $9A_1^2 - 8\beta^2 > 0$ (see [Appendix A.2](#)).

Using the polar representation of ϑ and the De Moivre's theorem [18], the Taylor series expansions of $\sigma_3 + \sigma_2/\sigma_3$ and $\sigma_3 - \sigma_2/\sigma_3$ can be written as

$$\sigma_3 + \sigma_2/\sigma_3 = 20\sqrt{3(3A_1^2 - 2\beta^2)} \cos(\theta/3) + \mathcal{O}(k^2h^2), \quad (54)$$

$$\sigma_3 - \sigma_2/\sigma_3 = 20\sqrt{3(3A_1^2 - 2\beta^2)} \sin(\theta/3)I + \mathcal{O}(k^2h^2), \quad (55)$$

where

$$\tan(\theta) = \frac{\sqrt{3(9A_1^2 - 8\beta^2)}}{9A_1(A_1^2 - \beta^2)}. \quad (56)$$

These expressions lead to the following Taylor expansions of the roots in Equations (45), (46) and (47)

$$w_{h,1}^2 = c_\star^2 k^2 \left[\frac{1}{h^2} \left(30A_1 + 20\sqrt{3(3A_1^2 - 2\beta^2)} \cos(\theta/3) \right) + \mathcal{O}(1) \right], \quad (57)$$

$$w_{h,2}^2 = c_\star^2 k^2 \left[\frac{1}{h^2} \left(30A_1 - 20\sqrt{3(3A_1^2 - 2\beta^2)} \cos((\theta + \pi)/3) \right) + \mathcal{O}(1) \right], \quad (58)$$

$$\begin{aligned} w_{h,3}^2 &= c_\star^2 k^2 \left[\frac{1}{h^2} \left(30A_1 - 20\sqrt{3(3A_1^2 - 2\beta^2)} \cos((\theta - \pi)/3) \right) + \mathcal{O}(1) \right] \\ &= c_\star^2 k^2 [1 + \mathcal{O}(k^2h^2)]. \end{aligned} \quad (59)$$

174 where it can be observed that Equation (59) corresponds to an approximation
175 of the dispersion relation of the wave equation whereas Equations (57) and (58)

176 correspond to two parasitic waves. As pointed out in Section 3.1, the objective
 177 of presenting the Taylor expansion of the roots is to distinguish the parasitic
 178 waves from the physical wave and not to analyse the accuracy of the roots as
 179 the element size h tends to zero.

180 To show that $30A_1 = 20\sqrt{3(3A_1^2 - 2\beta^2)} \cos((\theta - \pi)/3)$ (i.e. the root $w_{h,3}$
 181 corresponds to the physical wave), the roots of the polynomial $S(x) = 4x^3 -$
 182 $3x - \cos(\phi)$ are considered, namely $\cos(\phi/3)$, $\cos((2\pi + \phi)/3)$ and $\cos((4\pi +$
 183 $\phi)/3)$. As $x_\star = 3A_1(3A_1^2 - 2\beta^2)/(2|\vartheta|)$ is a root of $S(x)$ for $\phi = \theta - \pi$, it
 184 is clear that x_\star must be equal to one of the three roots $x_1 = \cos((\theta - \pi)/3)$,
 185 $x_2 = \cos((\theta + \pi)/3)$ and $x_3 = \cos((\theta + 3\pi)/3)$. The polar decomposition of
 186 ϑ implies $0 \leq \theta \leq \pi$ because $\sin \theta = \Im\{\vartheta\}/|\vartheta| \geq 0$. Therefore $x_1 \in (1/2, 1)$,
 187 $x_2 \in (-1/2, 1/2)$ and $x_3 \in (-1, -1/2)$. Finally, the positivity of β implies
 188 that $30A_1/(20\sqrt{3(3A_1^2 - 2\beta^2)}) = 1/(2\sqrt{1 - 2\beta^2/(9A_1^2)}) \geq 1/2$ and therefore
 189 $x_\star = x_1$, which implies that the third root $w_{h,3}$ corresponds to the physical
 190 wave.

191 4.2. Stability for the Leap-Frog scheme

The dispersion relations for the SEM with a Leap-Frog time integrator are
 given by

$$\frac{4}{\Delta t^2} \sin^2 \left(\frac{w_{h,l}^2 \Delta t}{2} \right) = w_{h,l}^2, \quad \text{for } l = 1, 2, 3. \quad (60)$$

192 The stability of the discrete scheme is controlled by the conditions

$$\sqrt{\max_{l=1,2,3} \left\{ \sup_{\omega \in [-1,1]} w_{h,l}^2(\omega), 0 \right\}} \leq \frac{2}{\Delta t}. \quad (61)$$

In this case, the maximum of the functions cannot be obtained explicitly so
 the strategy described in [1] is followed. Setting $kh = 2\pi K$ and $\lambda_l = h^2 w_{h,l}^2 / c_\star^2$,
 for $l = 1, 2, 3$, and using that $w_{h,l}^2$ are the roots of the characteristic polynomial,
 leads to

$$P(\lambda_l) = \lambda_l^3 - 90A_1\lambda_l^2 + 1800\beta^2\lambda_l - 4\omega^2 T(\lambda_l) = 0. \quad (62)$$

193 with $\omega = \sin(\pi K)$ and $T(\lambda_l) = \delta_1\lambda_l^2 + 60\delta_2\lambda_l + 1800\beta^2$.

Taking the derivative of Equation (62) with respect to K and noting that the maximum of λ_l , and consequently the maximum of $w_{h,l}^2$, is attained when $d\lambda_l/dK = 0$, leads to

$$\omega\sqrt{1-\omega^2}T(\lambda_l) = 0. \quad (63)$$

Equation (63) contains three classes of solutions. As discussed in Appendix A, the only two solutions relevant from the point of view of the stability of the Leap-Frog scheme are

$$\chi_2 = 15 \left(3A_1 + \sqrt{9A_1^2 - 8\beta^2} \right), \quad \chi_4 = \left[\tau_1 + \tau_3 + \frac{\tau_2}{\tau_3} \right], \quad (64)$$

194 where $\tau_i = \sigma_i(1)$ for $i = 1, 2, 3$.

The stability condition is therefore given by

$$\alpha = \frac{c_*\Delta t}{h} \leq \alpha_M, \quad (65)$$

with

$$\alpha_M = \frac{2}{\max\{\sqrt{\chi_2}, \sqrt{\chi_4}\}}. \quad (66)$$

195 It is worth noting that for a homogeneous medium the polynomial T , which
 196 reduces to the case presented in [1], has no real roots and there are only two
 197 classes of solutions. It can also be observed that the well known homogeneous
 198 stability condition $\alpha_M = 2/\sqrt{6(7 + \sqrt{29})} \approx 0.23$ (see Table 1) is recovered when
 199 $\beta = A_1 = \delta_1 = \delta_2 = 1$.

200 4.3. Numerical examples

Three numerical examples are considered to validate the stability condition derived in this Section and to illustrate that using a condition derived for the homogeneous case can lead to either unstable results or inefficient simulations. The domain $\Omega = [0, 1]$ is considered and the material parameters are defined as

$$\gamma(x) = \phi_1 + \phi_2 \sin(2\pi x/h + \phi_3), \quad \eta(x) = \psi_1 + \psi_2 \sin(2\pi x/h + \psi_3) \quad (67)$$

201 where the constants ϕ_i and ψ_i , for $i = 1, 2, 3$ are selected so that $\gamma(x_i) = \gamma_i$,
 202 $\gamma(x_{i,1}) = \gamma_{i,1}$, $\gamma(x_{i,2}) = \gamma_{i,2}$, $\eta(x_i) = \eta_i$, $\eta(x_{i,1}) = \eta_{i,1}$ and $\eta(x_{i,2}) = \eta_{i,2}$.

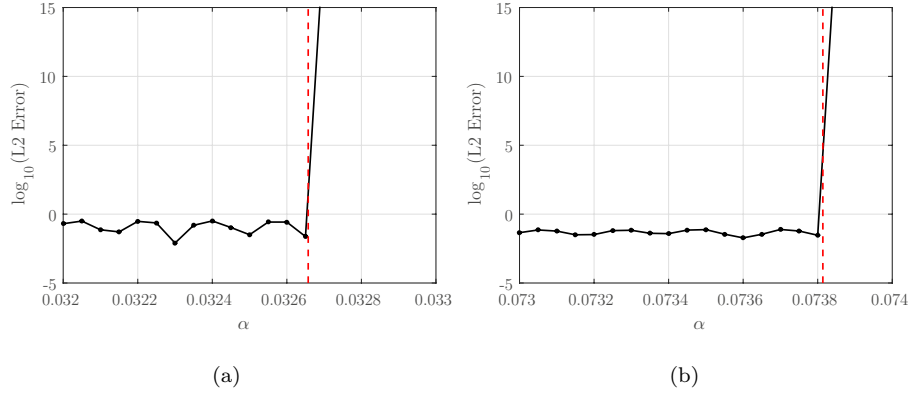


Figure 4: Relative error in the $\mathcal{L}^2(\Omega)$ norm as a function of $\alpha = c_* \Delta t / h$ for (a) $Q_{\gamma,1} = Q_{\gamma,2} = 10$, $Q_{\eta,1} = Q_{\eta,2} = 1/10$ and (b) $Q_{\gamma,1} = 1$, $Q_{\gamma,2} = 1/10$, $Q_{\eta,1} = Q_{\eta,2} = 1/10$. The discontinuous line represents the stability limit corresponding to α_M .

203 The analytical solution given in Equation (38) is again considered and the
 204 initial, boundary conditions and source term are derived from the exact solution
 205 as usually done in the method of manufactured solutions. In all the examples,
 206 the solution is advanced in time up to a final time $T = 10$ and the relative
 207 error in the $\mathcal{L}^2(\Omega)$ norm is measured. Analogously to the previous examples in
 208 Section 3.4, the goal is to evaluate the accuracy of the stability limit derived for
 209 cubic spectral elements with a periodic fluctuation of the material properties
 210 and not to study the accuracy of the numerical scheme.

211 The first example considers $\gamma_i = 10$, $\gamma_{i,1} = 1$, $\gamma_{i,2} = 1$, $\eta_i = 1$, $\eta_{i,1} = 10$
 212 and $\eta_{i,2} = 10$. The stability condition from Equation (66) is $\alpha_M \approx 0.03265$
 213 and it is given by the first term in the maximum in Equation (66). Figure 4
 214 (a) shows the relative error in the $\mathcal{L}^2(\Omega)$ norm as a function of the value of α
 215 considered to define the time step Δt for a uniform mesh with $h = 0.01$. It
 216 can be clearly observed that when the time step is defined by using a value of
 217 $\alpha \leq \alpha_M$ stability is guaranteed, whereas a value of $\alpha > \alpha_M$ leads to unstable
 218 results. In this example, if the time step is computed using the results derived
 219 from the homogeneous case, as detailed in Equation (36), the time step would
 220 be selected as $\Delta t \approx 2.15 \times 10^{-3}$ clearly leading to unstable results as it is more

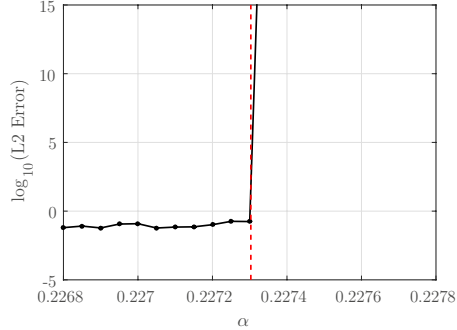


Figure 5: Relative error in the $\mathcal{L}^2(\Omega)$ norm as a function of $\alpha = c_*\Delta t/h$ for $\gamma_i = 1$, $\gamma_{i,1} = 1$, $\gamma_{i,2} = 10$, $\eta_i = 10$, $\eta_{i,1} = 10$ and $\eta_{i,2} = 1$. The discontinuous line represents the stability limit corresponding to α_M .

221 than two times higher than the bound derived for the heterogeneous case, i.e.
 222 $\Delta t \leq 8.78 \times 10^{-4}$.

223 The second example considers $\gamma_i = 1$, $\gamma_{i,1} = 1$, $\gamma_{i,2} = 10$, $\eta_i = 1$, $\eta_{i,1} = 10$
 224 and $\eta_{i,2} = 10$. The stability condition from Equation (66) is $\alpha_M \approx 0.073814$ and
 225 it is now given by the second term in the maximum in Equation (66). Figure 4
 226 (b) shows the relative error in the $\mathcal{L}^2(\Omega)$ norm as a function of the value of α
 227 considered to define the time step Δt for a uniform mesh with $h = 0.01$. Again,
 228 the results illustrate the validity of the stability limit found in this Section.
 229 In this example, if the time step is computed using the results derived from
 230 the homogeneous case ($\Delta t \approx 6.81 \times 10^{-3}$) unstable results are obtained as the
 231 stability limit induces a time step more than four times smaller, i.e. $\Delta t \leq$
 232 1.55×10^{-3} .

233 The last example considers a case where the time step computed using the
 234 homogeneous results leads to stable results but the simulation is less efficient
 235 than if the time step was computed from the heterogeneous bound presented in
 236 this Section. The material parameters are given by $\gamma_i = 1$, $\gamma_{i,1} = 1$, $\gamma_{i,2} = 10$,
 237 $\eta_i = 10$, $\eta_{i,1} = 10$ and $\eta_{i,2} = 1$. Figure 5 shows the relative error in the $\mathcal{L}^2(\Omega)$
 238 norm as a function of the value of α considered to define the time step Δt
 239 for a uniform mesh with $h = 0.01$. Once more, the validity of the proposed

240 stability limit is clearly demonstrated. In this case both terms in the maximum
 241 in Equation (66) have a similar value, namely $\chi_2 \approx 77.41$ and $\chi_4 \approx 75.19$. If the
 242 time step is computed using the results derived from the homogeneous case, the
 243 time step would be selected as $\Delta t \approx 2.15 \times 10^{-3}$, exactly the same as in the first
 244 example, leading to stable results here. When compared to the stability limit
 245 for the heterogeneous case (i.e. $\Delta t \approx 4.08 \times 10^{-3}$), the results reveal that the
 246 simulation using the time step computed from the homogeneous case results in
 247 almost twice the cost of the simulation with the time step computed from the
 248 heterogeneous stability limit.

249 5. Extensions

250 This Section briefly discusses three extensions of the analysis presented in
 251 detail for quadratic and cubic spectral elements in Sections 3 and 4 respectively.
 252 The extension to high-order polynomial approximations, larger periodicity of the
 253 material parameter fields and higher dimensions are considered.

254 5.1. Higher order polynomial approximations

255 The Von Neumann stability analysis described in previous sections can be
 256 extended to any order of the polynomial approximation. A detailed analysis,
 257 as presented for the quadratic and cubic case, is difficult due to the increase
 258 of the degree of the characteristic polynomial with the order of the polynomial
 259 approximation. However, with the aid of a symbolic package it is possible to
 260 obtain an exact expressions of the stability limit for a degree of approximation
 261 $p = 4$. For higher orders, it is always possible to obtain an accurate approx-
 262 imation of the stability limit by employing standard root finding algorithms
 263 (e.g. Newton-Raphson) to estimate the value of the roots of the characteristic
 264 polynomial.

Two examples are considered to validate the stability condition derived for
 $p = 4$. The domain $\Omega = [0, 1]$ is considered and the material parameters are

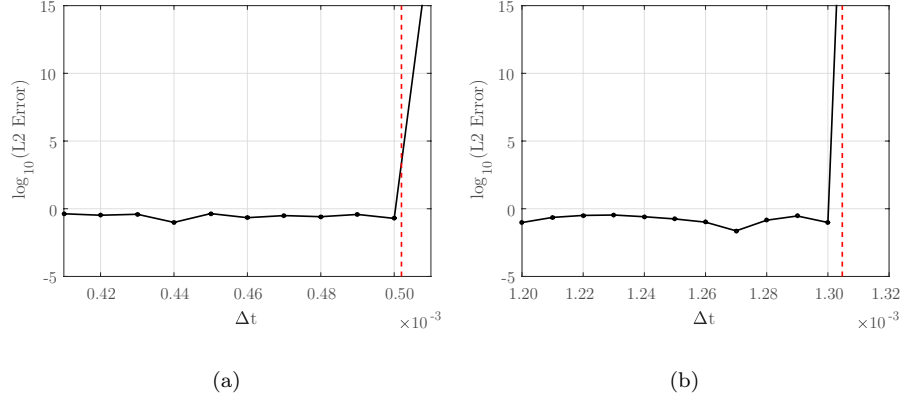


Figure 6: Relative error in the $\mathcal{L}^2(\Omega)$ norm as a function of Δt for (a) $\gamma_i = 10$, $\gamma_{i,1} = 1$, $\gamma_{i,2} = 1$, $\gamma_{i,3} = 10$, $\eta_i = 1$, $\eta_{i,1} = 10$, $\eta_{i,2} = 10$, $\eta_{i,3} = 1$ and (b) $\gamma_i = 4$, $\gamma_{i,1} = 2$, $\gamma_{i,2} = 1$, $\gamma_{i,3} = 5$, $\eta_i = 3$, $\eta_{i,1} = 6$, $\eta_{i,2} = 1$, $\eta_{i,3} = 4$. The discontinuous line represents the stability limit.

defined as

$$\gamma(x) = \phi_1 + \phi_2 \sin(2\pi x/h) + \phi_3 \cos(2\pi x/h) + \phi_4 \sin^2(2\pi x/h), \quad (68a)$$

$$\eta(x) = \psi_1 + \psi_2 \sin(2\pi x/h) + \psi_3 \cos(2\pi x/h) + \psi_4 \sin^2(2\pi x/h) \quad (68b)$$

265 where the constants ϕ_i and ψ_i , for $i = 1, \dots, 4$, are selected so that $\gamma(x_i) = \gamma_i$,
 266 $\gamma(x_{i,k}) = \gamma_{i,k}$, $\eta(x_i) = \eta_i$ and $\eta(x_{i,k}) = \eta_{i,k}$ for $k = 1 \dots, 3$. The analytical
 267 solution given in Equation (38) is again considered.

268 The first example considers $\gamma_i = 10$, $\gamma_{i,1} = 1$, $\gamma_{i,2} = 1$, $\gamma_{i,3} = 10$, $\eta_i = 1$,
 269 $\eta_{i,1} = 10$, $\eta_{i,2} = 10$ and $\eta_{i,3} = 1$. The stability condition derived with the aid
 270 of a symbolic package is $\Delta t \approx 5.0197 \times 10^{-3}$. Figure 6 (a) shows the relative
 271 error in the $\mathcal{L}^2(\Omega)$ norm as a function of the time step Δt for a uniform mesh
 272 with $h = 0.01$. A second example is considered with $\gamma_i = 4$, $\gamma_{i,1} = 2$, $\gamma_{i,2} = 1$,
 273 $\gamma_{i,3} = 5$, $\eta_i = 3$, $\eta_{i,1} = 6$, $\eta_{i,2} = 1$ and $\eta_{i,3} = 4$. The stability condition is
 274 $\Delta t \approx 1.3047 \times 10^{-3}$. Figure 6 (b) shows the relative error in the $\mathcal{L}^2(\Omega)$ norm as
 275 a function of the time step Δt .

276 In both cases, the results demonstrate the validity of the stability limit
 277 obtained for quartic spectral elements.

278 *5.2. Larger periodicity of the material parameter fields*

279 The extension to problems involving material properties whose periodicity
 280 is larger than a single element is also possible using the Von Neumann analysis
 281 described in previous sections. Once more, the difficulty increases due to the
 282 higher degree of the characteristic polynomial. With the aid of a symbolic pack-
 283 age, it is possible to obtain an exact expressions of the stability limit only for
 284 quadratic spectral elements and periodicity equals to $2h$, where h is the char-
 285 acteristic element size. For higher orders approximations with periodicity $2h$ or
 286 for larger periodicities, it is always possible to obtain an accurate approximation
 287 of the stability limit by employing standard root finding algorithms.

288 Two examples are considered to validate the stability condition derived for
 289 quadratic spectral elements and periodicity $2h$. The domain $\Omega = [0, 1]$ is con-
 290 sidered and the material parameters are defined in Equation (68). In this case,
 291 the constants ϕ_i and ψ_i , for $i = 1, \dots, 4$, are selected so that $\gamma(x_1^{2k+1}) = \gamma_1^{2k+1}$,
 292 $\gamma(x_{i,1}^{2k+1}) = \gamma_{i,1}^{2k+1}$, $\gamma(x_1^{2k}) = \gamma_1^{2k}$, $\gamma(x_{i,1}^{2k}) = \gamma_{i,1}^{2k}$, $\eta(x_1^{2k+1}) = \eta_1^{2k+1}$, $\eta(x_{i,1}^{2k+1}) =$
 293 $\eta_{i,1}^{2k+1}$, $\eta(x_1^{2k}) = \eta_1^{2k}$ and $\eta(x_{i,1}^{2k}) = \eta_{i,1}^{2k}$ where the superscript is used to specify
 294 odd and even element numbers.

295 The first example considers $\gamma_1^{2k+1} = 10$, $\gamma_{i,1}^{2k+1} = 1$, $\gamma_1^{2k} = 1$, $\gamma_{i,1}^{2k} = 10$,
 296 $\eta_1^{2k+1} = 1$, $\eta_{i,1}^{2k+1} = 10$, $\eta_1^{2k} = 10$ and $\eta_{i,1}^{2k} = 1$. The stability condition derived
 297 with the aid of a symbolic package is $\Delta t \approx 1.7167 \times 10^{-3}$. Figure 7 (a) shows
 298 the relative error in the $\mathcal{L}^2(\Omega)$ norm as a function of the time step Δt for a
 299 uniform mesh with $h = 0.01$. A second example is considered with $\gamma_1^{2k+1} = 4$,
 300 $\gamma_{i,1}^{2k+1} = 2$, $\gamma_1^{2k} = 1$, $\gamma_{i,1}^{2k} = 5$, $\eta_1^{2k+1} = 3$, $\eta_{i,1}^{2k+1} = 6$, $\eta_1^{2k} = 1$ and $\eta_{i,1}^{2k} = 4$. The
 301 stability condition is $\Delta t \approx 3.6820 \times 10^{-3}$. Figure 7 (b) shows the relative error
 302 in the $\mathcal{L}^2(\Omega)$ norm as a function of the time step Δt .

303 The results demonstrate the validity of the stability limit obtained for a
 304 larger periodicity of the material parameter fields with quadratic approximation.
 305 It is also worth noting that the magnitude of the material parameters at the
 306 mesh nodes is the same as in the example with $p = 4$ spectral elements. However,
 307 it is clear from the numerical results in Figures 6 and 7 that the stability limit
 308 is significantly different, being more restrictive for high order approximations.

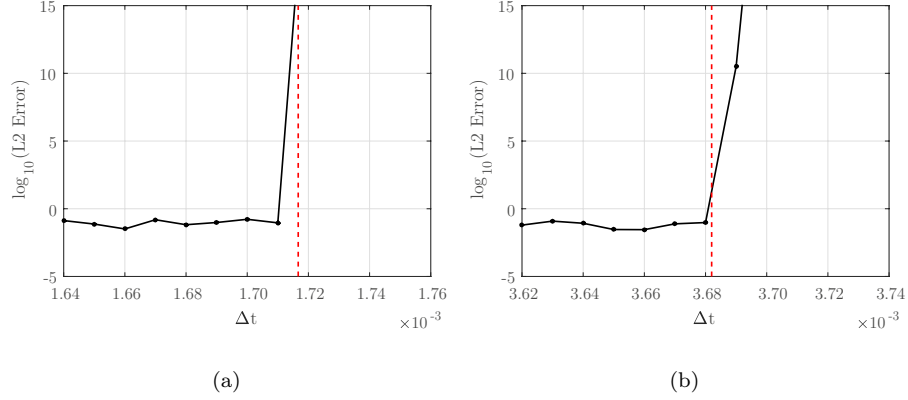


Figure 7: Relative error in the $\mathcal{L}^2(\Omega)$ norm as a function of Δt for (a) $\gamma_1^{2k+1} = 10$, $\gamma_{i,1}^{2k+1} = 1$, $\gamma_1^{2k} = 1$, $\gamma_{i,1}^{2k} = 10$, $\eta_1^{2k+1} = 1$, $\eta_{i,1}^{2k+1} = 10$, $\eta_1^{2k} = 10$, $\eta_{i,1}^{2k} = 1$ and (b) $\gamma_1^{2k+1} = 4$, $\gamma_{i,1}^{2k+1} = 2$, $\gamma_1^{2k} = 1$, $\gamma_{i,1}^{2k} = 5$, $\eta_1^{2k+1} = 3$, $\eta_{i,1}^{2k+1} = 6$, $\eta_1^{2k} = 1$, $\eta_{i,1}^{2k} = 4$. The discontinuous line represents the stability limit.

309 5.3. Higher dimensions

310 Following the methodology described in [1, Section 12.2] (and originally de-
 311 rived in [19, 20]) for homogeneous materials, the results presented in this paper
 312 for one-dimensional problems can be easily extended to higher dimensions when
 313 the functions that describe the material properties can be written as a tensor
 314 product of one-dimensional functions.

Assuming the following decomposition in d dimensions:

$$\eta(x_1, \dots, x_d) = \prod_{k=1}^d \eta^k(x_k) \quad \gamma(x_1, \dots, x_d) = \prod_{k=1}^d \gamma^k(x_k), \quad (69)$$

where $\eta^k(x_k)$ and $\gamma^k(x_k)$ denote the one-dimensional material field in the x_k direction, it can be shown, using an extension of the original method described in previous sections, that the roots of the characteristic equation correspond to the sum of the roots of the one-dimensional characteristic equations corresponding to one-dimensional material fields

$$w_{h,l_d}^2(\omega) = \sum_{k=1}^d w_{h,l,k}^2(\omega), \quad l = 1, \dots, p, \quad k = 1, \dots, d \quad (70)$$

where $w_{h,l,k}(\omega)$ denotes a root of Equation (21) with parameter fields $\eta^k(x_k)$ and $\gamma^k(x_k)$. The stability limit can be written as

$$\Delta t \leq \frac{2}{\sqrt{\max_{1 \leq l \leq p} \left\{ \sup_{\omega \in [-1,1]} \left(\sum_{k=1}^d w_{h,l,k}^2(\omega) \right), 0 \right\}}}. \quad (71)$$

315 With the aid of a symbolic package, it is possible to find the supremum of
 316 Equation (71) for quadratic elements in two dimensions. For higher orders in
 317 two dimensions, or higher dimensions, the supremum can be found by using
 318 standard root finding algorithms.

Alternatively, an upper bound of the roots of the characteristic polynomial corresponding to the multi-dimensional problem can be expressed as

$$\max_{1 \leq l \leq p} \left\{ \sup_{\omega \in [-1,1]} \left(\sum_{k=1}^d w_{h,l,k}^2(\omega) \right), 0 \right\} \leq \sum_{k=1}^d \left(\max_{1 \leq l \leq p} \left\{ \sup_{\omega \in [-1,1]} w_{h,l,k}^2(\omega), 0 \right\} \right) \quad (72)$$

and a conservative stability limit, using results from the one-dimensional analysis, reads

$$\Delta t \leq \frac{2}{\sqrt{\sum_{k=1}^d \left(\max_{1 \leq l \leq p} \left\{ \sup_{\omega \in [-1,1]} w_{h,l,k}^2(\omega), 0 \right\} \right)}}. \quad (73)$$

319
 320 It is worth noting that, if Equation (72) is an equality, then the stabil-
 321 ity limit derived from a one-dimensional analysis is exact. Furthermore, when
 322 $w_{h,l,1} = \dots = w_{h,l,d}$, for $l = 1, \dots, p$, the stability limit in d dimensions is ob-
 323 tained by dividing the one-dimensional stability limit by \sqrt{d} . A particular case
 324 corresponds to a medium where the material properties in each dimension co-
 325 incide, that is $\eta^1(x_1) = \dots = \eta^d(x_d)$ and $\gamma^1(x_1) = \dots = \gamma^d(x_d)$. This confirms
 326 the results detailed in [1] for a homogeneous medium.

327 In the case of non-tensorised material properties (i.e. when Equation (69) is
 328 not verified), one-dimensional results cannot be employed and the Von Neumann
 329 stability analysis must be repeated for the full multi-dimensional problem.

Two examples in two dimensions are considered to validate the stability limits derived for the multi-dimensional case with quadratic spectral elements.

The domain $\Omega = [0, 1]^2$ is considered and the material parameters are defined, similarly to the one-dimensional case with $p = 2$ presented in Section 3, as

$$\gamma^1(x) = \gamma_i^1 + (\gamma_{i,1}^1 - \gamma_i^1) \sin^2(\pi x/h), \quad \eta^1(x) = \eta_i^1 + (\eta_{i,1}^1 - \eta_i^1) \sin^2(\pi x/h), \quad (74a)$$

$$\gamma^2(x) = \gamma_i^2 + (\gamma_{i,1}^2 - \gamma_i^2) \sin^2(\pi x/h), \quad \eta^2(x) = \eta_i^2 + (\eta_{i,1}^2 - \eta_i^2) \sin^2(\pi x/h). \quad (74b)$$

330 The first example considers a material with $\gamma_i^1 = 1$, $\gamma_{i,1}^1 = 3$, $\gamma_i^2 = 2$, $\gamma_{i,1}^2 = 4$,
 331 $\eta_i^1 = 2$, $\eta_{i,1}^1 = 6$, $\eta_i^2 = 4$ and $\eta_{i,1}^2 = 8$. Figure 8 (a) shows the $\mathcal{L}^2(\Omega)$ norm of the
 332 solution at time $T = 10$ as a function of Δt . The red and blue discontinuous
 333 lines represent the stability limit of Equations (71) and (73) respectively. It can
 334 be clearly observed that the stability limit derived for the multi-dimensional
 335 problem is exact whereas the stability limit derived from the one-dimensional
 336 analysis is conservative due to the bound introduced in Equation (72). A second
 337 example is considered using a medium that leads to an equality in Equation (72),
 338 meaning that the stability limit in Equation (73) is exact. Figure 8 (b) shows
 339 the $\mathcal{L}^2(\Omega)$ norm of the solution at time $T = 10$ as a function of Δt for a material
 340 with $\gamma_i^1 = 1$, $\gamma_{i,1}^1 = 3$, $\gamma_i^2 = 1$, $\gamma_{i,1}^2 = 3$, $\eta_i^1 = 2$, $\eta_{i,1}^1 = 6$, $\eta_i^2 = 2$ and $\eta_{i,1}^2 = 6$. In
 341 this case the red and blue lines are overlapped as the two stability limits given
 342 by Equations (71) and (73) coincide.

343 6. Numerical examples in randomly fluctuating media

344 This Section presents a number of examples of wave propagation in ran-
 345 domly heterogeneous media. The periodicity hypothesis for the material prop-
 346 erties does not hold and therefore, the stability analyses in Sections 3 and 4
 347 are theoretically not valid. However, the objective is to show that the criteria
 348 developed in this paper still provide reasonable estimates for the stability in
 349 more complex scenarios.

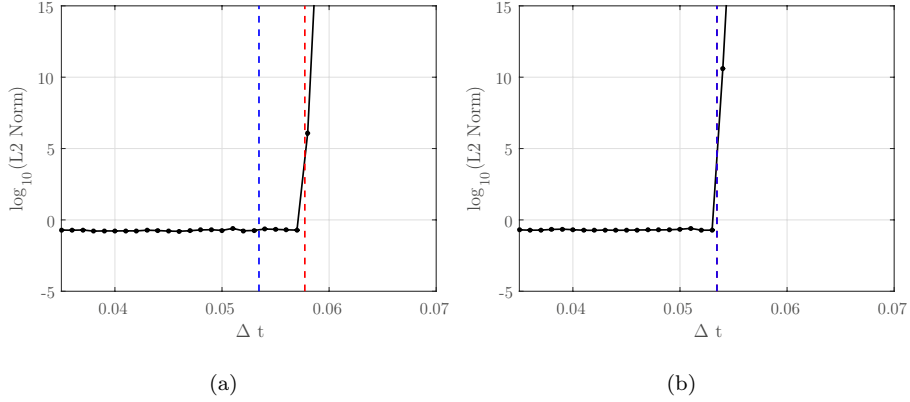


Figure 8: $\mathcal{L}^2(\Omega)$ norm of the solution at time $T = 10$ as a function of Δt for (a) $\gamma_i^1 = 1$, $\gamma_{i,1}^1 = 3$, $\gamma_i^2 = 2$, $\gamma_{i,1}^2 = 4$, $\eta_i^1 = 2$, $\eta_{i,1}^1 = 6$, $\eta_i^2 = 4$, $\eta_{i,1}^2 = 8$ and (b) $\gamma_i^1 = 1$, $\gamma_{i,1}^1 = 3$, $\gamma_i^2 = 1$, $\gamma_{i,1}^2 = 3$, $\eta_i^1 = 2$, $\eta_{i,1}^1 = 6$, $\eta_i^2 = 2$, $\eta_{i,1}^2 = 6$. The red and blue discontinuous lines represent the stability limit of Equations (71) and (73) respectively. In (b), the red and blue lines overlap.

350 *6.1. Stability of wave propagation in quasi-periodic randomly heterogeneous me-*
 351 *dia*

352 The propagation of a wave in $\Omega = [0, 1]$ is considered. The domain is
 353 meshed with 20 elements of length $h = 0.05$. The material properties are
 354 randomly fluctuating within the elements, but always take the same value at
 355 the vertices (see two examples in Figure 9). More specifically, the parame-
 356 ters at all the vertices are $\eta_i = 5$ and $\gamma_i = 2$, whereas within the elements
 357 (one node for quadratic polynomials, and two nodes for cubic polynomials)
 358 they are realisations of independent log-normal random variables with averages
 359 $\underline{\eta} = \mathbb{E}[\eta(x)] = 5$ and $\underline{\gamma} = \mathbb{E}[\gamma(x)] = 2$ and variances $\sigma_{\underline{\eta}}^2 = \mathbb{E}[(\eta(x) - \underline{\eta})^2] = 32$
 360 and $\sigma_{\underline{\gamma}}^2 = \mathbb{E}[(\gamma(x) - \underline{\gamma})^2] = 2$. Although there is no analytical solution for this
 361 problem, the same boundary conditions, initial conditions and source term as in
 362 the examples of Section 3.4 are considered. In all the examples, the solution is
 363 advanced in time up to a final time $T = 10$ and the $\mathcal{L}^2(\Omega)$ norm of the solution
 364 $u(x, T)$ is measured.

The stability limits of Equation (32) and (66) are modified slightly because the equivalent velocity c_* is not constant throughout the elements. The stability

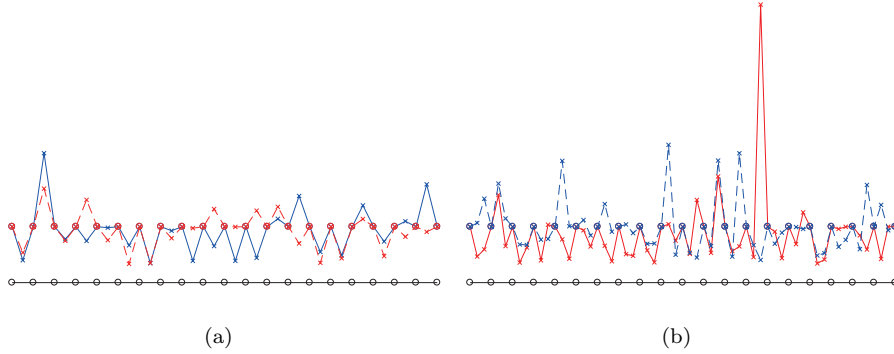


Figure 9: Two realisations of the quasi-periodic randomly fluctuating properties for (a) quadratic and (b) cubic polynomials. The solid and dashed fluctuating lines represent the two realisations, respectively, and the lower line represents the mesh elements. The circles indicate the position of the vertices.

limit is therefore taken directly in terms of the time step as

$$\Delta t \leq h \min \left(\frac{\alpha_M}{c_\star} \right), \quad (75)$$

365 where the minimum is taken over all elements of the mesh, and α_M is given
366 by Equation (32) with element-dependent β and δ , and (66) with element-
367 dependent β , δ_1 , δ_2 and A_1 , for quadratic and cubic polynomials, respectively.
368 As only 20 elements are considered, there is a strong variability of the time
369 step (and the actual stability limit) computed for different realisations of the
370 material properties. Figure 10 presents the probability density function (PDF)
371 of the time step Δt computed with Equation (75) for different realisations of the
372 20 elements-long bar. As this PDF depends on the length, three different lengths
373 are considered. The estimations of the PDFs are obtained through Monte Carlo
374 sampling with 100,000 realisations and 50 bins for the histogram. As expected,
375 it can be observed that the stability limit becomes more stringent for longer
376 domains, for both quadratic and cubic polynomials. It is also interesting to
377 note that the heterogeneous stability limit is systematically higher than the
378 homogeneous stability limit (for this particular setting), which means that using
379 the homogeneous criterion would yield an unnecessary higher computational
380 cost.

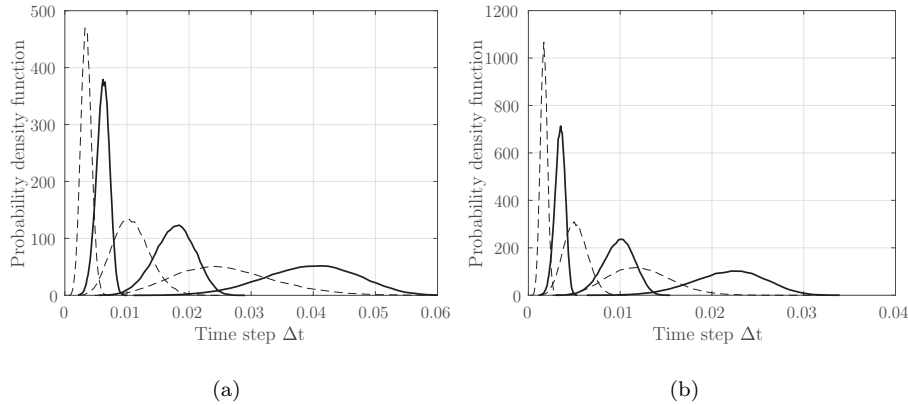


Figure 10: Probability density function of the time step Δt computed with Equation (75) for (a) quadratic and (b) cubic polynomials. The three solid lines correspond to lengths of 10, 20 and 50 elements respectively (the smallest Δt corresponds to the longest domain) and the thin dashed line corresponds to the homogeneous stability criterion of Equation (36) for the same lengths.

381 Figure 11 presents stability results, obtained for three different realisations
 382 of the 20-element domain described above. As expected, the stability criterion
 383 is not as precise as in the periodic case, since the theoretical derivation is not
 384 applicable, but it is interesting to note that, for the three realisations considered,
 385 the stability constant is both conservative and accurate. It is conservative in
 386 the sense that instability seems to arise for larger time steps than predicted by
 387 the stability coefficient. It is accurate in the sense that there is a very small
 388 difference between the time step predicted and the time step for which instability
 389 arises. This stability limit is compared to the homogeneous stability criterion of
 390 Equation (36), which confirms the previous observation that the homogeneous
 391 criterion is systematically overly conservative for this particular setting.

Finally, the relative distance to instability provided by the stability limit in Equation (75) is computed for 1,000 samples of 20 elements of the bar of the PDF. This relative distance is defined as

$$DtI = 2 \frac{\Delta t_{\text{instab}} - \Delta t}{\Delta t_{\text{instab}} + \Delta t}, \quad (76)$$

392 where Δt_{instab} is the time step at which instability emerges for a given sample.

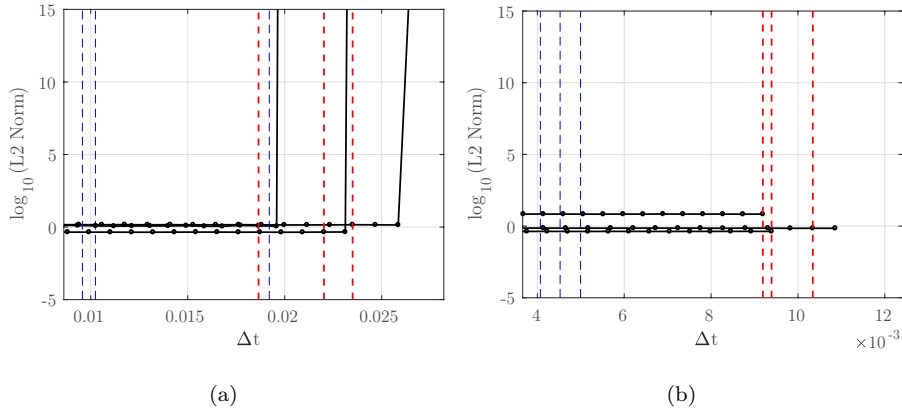


Figure 11: $\mathcal{L}^2(\Omega)$ norm of the solution at time $T = 10$ as a function of Δt for three realisations of a quasi-periodic randomly fluctuating case with (a) quadratic and (b) cubic polynomials. The discontinuous red line represents the heterogeneous stability criterion of Equation (75), and the discontinuous blue line correspond to the homogeneous stability criterion of Equation (36).

393 This coefficient is clearly expected to be small if the stability limit is accurate
 394 and it is expected to be positive if the stability limit is conservative. The
 395 PDF for the relative distance to instability is approximated using 50 bins and
 396 represented in Figure 12. It is remarkable that, even though the theory is not
 397 directly applicable because the material properties are not periodic, the stability
 398 criterion is still both accurate and conservative. In particular, it is much more
 399 accurate than the homogeneous stability limit estimated with Equation (36). It
 400 is interesting to note that, even though it is mostly conservative, the homoge-
 401 neous limit does induce instability in some cases (i.e. the dashed curve does not
 402 vanish completely for negative values of the instability limit in Figure 12), at
 403 least in the quadratic case.

404 6.2. Stability of wave propagation in randomly heterogeneous media

405 The following set of numerical examples considers the wave propagation in
 406 a randomly heterogeneous medium. The constraint of having the same value
 407 of the material properties in the mesh vertices is removed (see two examples

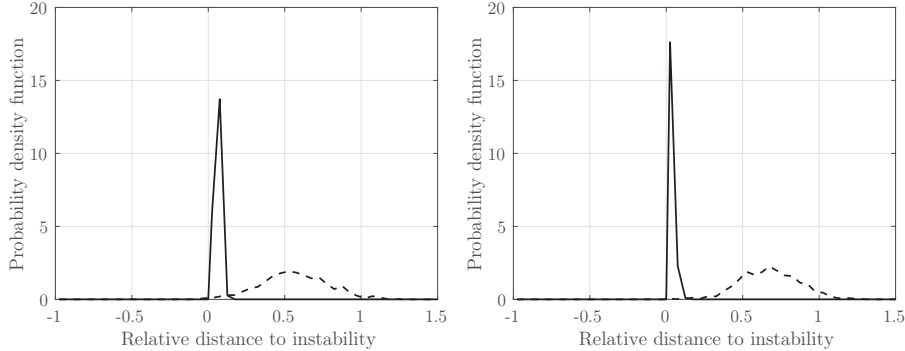


Figure 12: Probability density function of the relative distance (in time) to instability for quadratic (left figure) and cubic polynomials (right figure). The solid lines represent the heterogeneous stability criterion of Equation (75), and the discontinuous lines correspond to the homogeneous stability criterion of Equation (36).

408 in Figure 13) and the applicability of the stability limits derived for periodic
 409 material properties is studied numerically.

410 The parameters are realisations of statistically homogeneous random fields
 411 with log-normal first-order marginal densities with averages $\underline{\eta} = \mathbb{E}[\eta(x)] = 5$ and
 412 $\underline{\gamma} = \mathbb{E}[\gamma(x)] = 2$ and variances $\sigma_{\eta}^2 = \mathbb{E}[(\eta(x) - \underline{\eta})^2] = 32$ and $\sigma_{\gamma}^2 = \mathbb{E}[(\gamma(x) -$
 413 $\underline{\gamma})^2] = 2$. As in the previous examples, the random fields of the two parameters
 414 are assumed independent. The solution is advanced in time up to a final time
 415 $T = 10$ and the $\mathcal{L}^2(\Omega)$ norm of the solution $u(T)$ is measured.

416 Computing the solution for 1000 realisations of the random fields, either
 417 with quadratic or cubic polynomials, it is possible to construct the PDF of the
 418 relative distance to instability, as in Equation (76). These PDF are represented
 419 in Figure 14. Contrary to the case of the quasi-periodic fields, the heteroge-
 420 neous stability criterion of Equation (75) is not always conservative, although
 421 it remains rather accurate. Comparing this limit to the homogeneous stabil-
 422 ity criterion of Equation (36), it is not very clear which estimate is the most
 423 appropriate for a given simulation. Indeed, in most cases, conservatism would
 424 probably be preferred over precision. Indeed, running into instability forces the
 425 user to restart the simulation completely, while a slightly over-constrained time

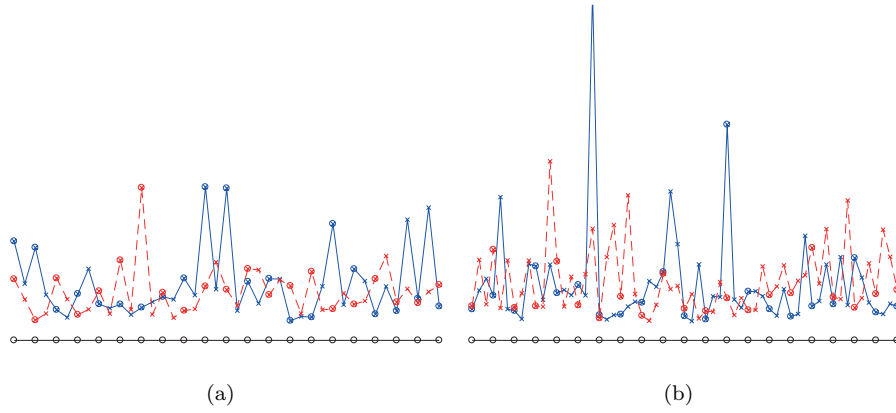


Figure 13: Two realisations of the non-periodic randomly-fluctuating properties for (a) quadratic and (b) cubic polynomials. The solid and dashed fluctuating lines represent the two realisations, respectively, and the lower line represents the mesh elements. The circles indicate the position of the vertices.

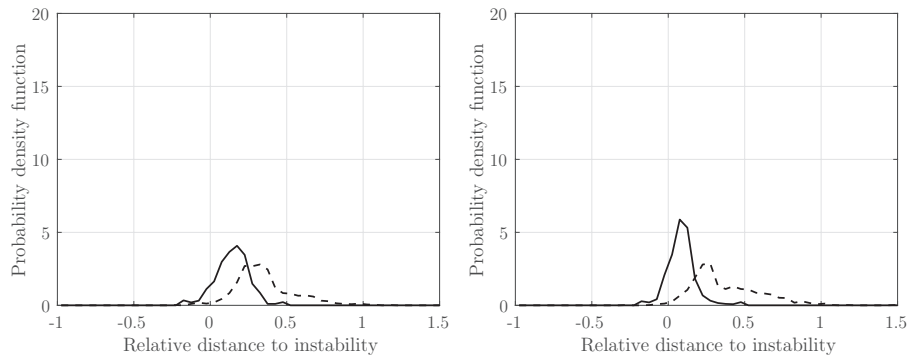


Figure 14: Probability density function of the relative distance (in time) to instability for quadratic (left figure) and cubic polynomials (right figure). The solid lines represent the heterogeneous stability criterion of Equation (75), and the discontinuous lines correspond to the homogeneous stability criterion of Equation (36).

426 step only means a longer simulation time. This conclusion remains the same for
 427 both quadratic and cubic polynomials.

428 *6.3. Influence of correlation length*

429 Finally, correlated random fields for the parameters are considered, instead
430 of the white noise that was considered in previous examples with randomly
431 fluctuating material properties. The first-order marginal densities of the random
432 fields are the same as in the previous section. In addition, triangular power
433 density spectra is considered, with correlation length $\ell_c = h$ and $\ell_c = 3h$. From
434 these random models, realisations can be drawn (using for instance the spectral
435 representation method [21]) to obtain values of the material parameters at the
436 vertices and at the interior nodes. Computing the solution for 1,000 realisations
437 of the random fields, either with quadratic or cubic polynomials, the PDFs of the
438 relative distance to instability, as in Equation (76), are displayed in Figure 15.
439 To better analyse the results, the results reported in Figure 14, which formally
440 corresponds to $\ell_c = 0$, should be also considered. Similarly to the examples
441 with randomly fluctuating material properties, the heterogeneous criterion is
442 overall less conservative and more precise than the homogeneous criterion. As
443 expected, the two curves are closer when the correlation length increases, since
444 this corresponds to material properties being close to a homogeneous medium.

445 **7. Concluding remarks**

446 The stability of an explicit time marching algorithm for the spectral ele-
447 ment method in a medium with periodically fluctuating material parameters
448 has been discussed. A detailed Von Neumann stability analysis is presented for
449 quadratic and cubic polynomial approximations under the assumption of peri-
450 odic heterogeneous media with period equal to the characteristic element size.
451 The theoretical stability limits are demonstrated to be valid using numerical
452 examples. More important, the analysis reveals the origin of instabilities that
453 are often observed when the stability limit derived for homogeneous materials
454 is adapted by simply changing the velocity of the wave to account for the ma-
455 terial heterogeneity. The numerical examples show that adapting homogeneous

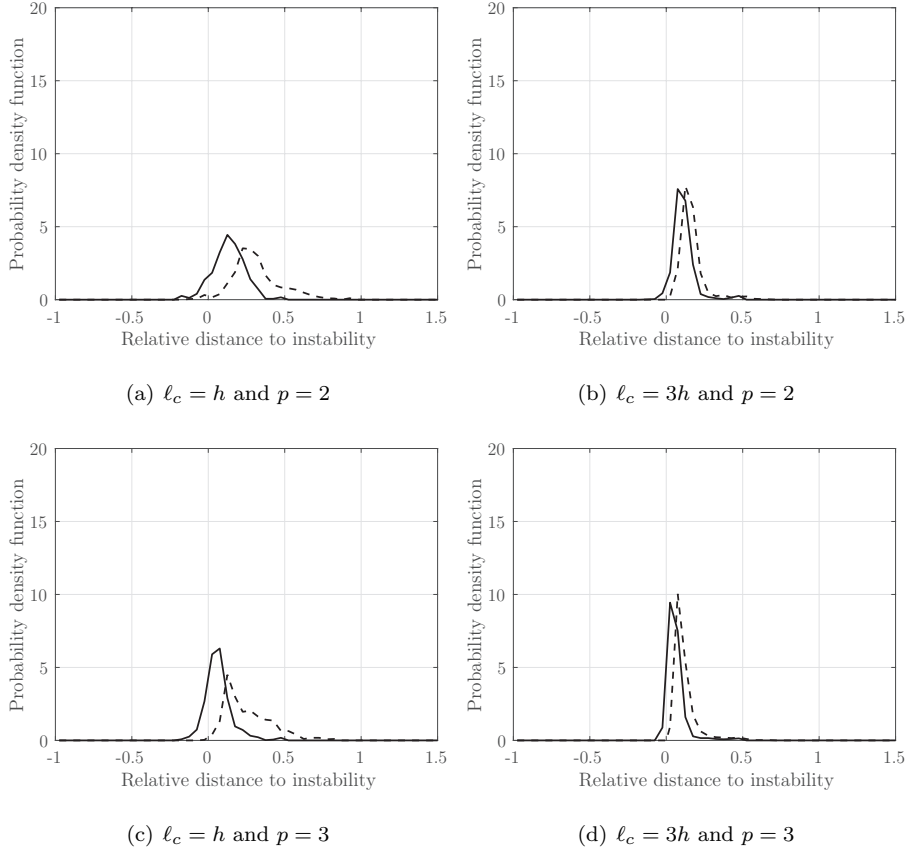


Figure 15: Probability density function of the relative distance (in time) to instability for 1000 realisations of correlated samples. The solid lines represent the heterogeneous stability criterion of Equation (75) and the discontinuous lines correspond to the homogeneous stability criterion of Equation (36).

456 formulae for heterogeneous media leads to either instability or to unnecessary
 457 increased computational resources.

458 Extensions of the results derived for quadratic and cubic one-dimensional
 459 spectral elements are discussed, including higher order approximations, differ-
 460 ent periodicity of the material parameters and higher dimensions. The main
 461 limitation of the analysis presented here is that exact formulas can only be de-
 462 rived when the degree of the characteristic polynomial is low (i.e. moderate
 463 polynomial orders of approximation, moderate period of the material parame-

464 ters compared to the element sizes), despite the methodology is still applicable
465 when combined with a root finding algorithm.

466 Extensive numerical results demonstrate the validity of the new stability
467 limits derived for heterogeneous materials with periodic fluctuation. In addition,
468 further numerical experiments of the stability for randomly fluctuating material
469 properties are presented. These numerical experiments reveal that the stability
470 limits derived for periodically fluctuating material properties are precise when
471 the material parameters take the same value at the vertices of the mesh. In
472 contrast, for fully randomly fluctuating material properties its accuracy is lower.

473 **Acknowledgements**

474 The authors would like to acknowledge the support provided by Centrale-
475 Supélec and the Erasmus+ programme for an invitation of the first author to
476 CentraleSupélec and the second author to Swansea University respectively. The
477 first author also gratefully acknowledges the financial support provided by the
478 Sêr Cymru National Research Network for Advanced Engineering and Materials,
479 United Kingdom.

480 **References**

- 481 [1] G. Cohen, Higher-order numerical methods for transient wave equations,
482 Scientific Computation, Springer, 2001.
- 483 [2] J. D. De Basabe, M. K. Sen, Grid dispersion and stability criteria of some
484 common finite-element methods for acoustic and elastic wave equations,
485 Geophysics 72 (6) (2007) T81–T95.
- 486 [3] J. D. De Basabe, M. K. Sen, Stability of the high-order finite elements
487 for acoustic or elastic wave propagation with high-order time stepping,
488 Geophysical Journal International 181 (2010) 577–590.

- 489 [4] C. Agut, J. Diaz, Stability analysis of the interior penalty discontinuous
490 Galerkin method for the wave equation, *ESAIM: Mathematical Modelling
491 and Numerical Analysis* 47 (3) (2013) 903–932.
- 492 [5] W. Mulder, E. Zhebel, S. Minisini, Time-stepping stability of continuous
493 and discontinuous finite-element methods for 3-d wave propagation, *Geo-
494 physical Journal International* 196 (2) (2014) 1123–1133.
- 495 [6] Y. Maday, E. M. Ronquist, Optimal error analysis of spectral methods with
496 emphasis on non-constant coefficients and deformed geometries, ICASE
497 Report 89-56, NASA Langley Research Center (1989).
- 498 [7] G. Seriani, E. Priolo, Spectral element method for acoustic wave simulation
499 in heterogeneous media, *Finite elements in analysis and design* 16 (3) (1994)
500 337–348.
- 501 [8] D. Komatitsch, S. Tsuboi, J. Tromp, The spectral-element method in seis-
502 mology, in: A. Levander, G. Nolet (Eds.), *Seismic Earth: Array Analysis
503 of Broadband Seismograms*, Vol. 157 of Geophysical Monograph, American
504 Geophysical Union, 2005, pp. 205–228.
- 505 [9] E. Casarotti, M. Stupazzini, S. J. Lee, D. Komatitsch, A. Piersanti,
506 J. Tromp, CUBIT and seismic wave propagation based upon the spectral-
507 element method: an advanced unstructured mesher for complex 3D geolog-
508 ical media, in: M. L. Brewer, D. Marcum (Eds.), *Proceedings of the 16th
509 International Meshing Roundtable*, no. 5B, Springer, 2008, pp. 579–597.
- 510 [10] P. Cupillard, E. Delavaud, G. Burgos, G. Festa, J.-P. Vilotte, Y. Capdeville,
511 J.-P. Montagner, RegSEM: a versatile code based on the spectral element
512 method to compute seismic wave propagation at the regional scale, *Geo-
513 physical Journal International* 188 (3) (2012) 1203–1220.
- 514 [11] K. C. Meza Fajardo, Numerical simulation of wave propagation in un-
515 bounded elastic domains using the spectral element method, Ph.D. thesis,
516 Università degli Studi di Pavia, Italy (2007).

- 517 [12] D. Komatitsch, J.-P. Vilotte, R. Vai, J. M. Castillo-Covarrubias, F. J.
518 Sánchez-Sesma, The spectral element method for elastic wave equations
519 – application to 2-D and 3-D seismic problems, *International Journal for*
520 *Numerical Methods in Engineering* 45 (9) (1999) 1139–1164.
- 521 [13] I. Mazzieri, M. Stupazzini, R. Guidotti, C. Smerzini, SPEED: SPectral EL-
522 ements in Elastodynamics with Discontinuous Galerkin: a non-conforming
523 approach for 3D multi-scale problems, *International Journal for Numerical*
524 *Methods in Engineering* 95 (12) (2013) 991–1010.
- 525 [14] A. T. Patera, A spectral element method for fluid dynamics: laminar flow
526 in a channel expansion, *Journal of Computational Physics* 54 (3) (1984)
527 468–488.
- 528 [15] G. Karniadakis, S. Sherwin, *Spectral/hp element methods for computa-*
529 *tional fluid dynamics*, Oxford University Press, 2013.
- 530 [16] R. J. LeVeque, Wave propagation algorithms for multidimensional hyper-
531 bolic systems, *Journal of Computational Physics* 131 (2) (1997) 327–353.
- 532 [17] L. Fezoui, S. Lanteri, S. Lohrengel, S. Piperno, Convergence and stability
533 of a discontinuous Galerkin time-domain method for the 3D heterogeneous
534 Maxwell equations on unstructured meshes, *ESAIM: Mathematical Mod-*
535 *elling and Numerical Analysis* 39 (6) (2005) 1149–1176.
- 536 [18] T. Nagell, *Introduction to number theory*, Wiley, 1951.
- 537 [19] N. Tordjman, *Éléments finis d’ordre élevé avec condensation de masse pour*
538 *l’équation des ondes*, Ph.D. thesis, Université Paris IX-Dauphine, Paris,
539 France (1995).
- 540 [20] S. Fauqueux, *Modélisation de la propagation d’ondes en milieu élastique par*
541 *éléments finis mixtes avec condensation de masse*, Ph.D. thesis, Université
542 Paris IX-Dauphine, Paris, France (2003).

543 [21] M. Shinozuka, G. Deodatis, Simulation of stochastic processes by spectral
 544 representation, Applied Mechanics Reviews 44 (4) (1991) 191–205.

545 **Appendix A. Solutions of Equation (63)**

546 The three classes of solutions of Equation (63) and their relevance to the
 547 stability of the Leap-Frog scheme are discussed in this Appendix.

548 *Appendix A.1. Solutions corresponding to $\omega = 0$*

Introducing $\omega = 0$ into the characteristic polynomial of Equation (62), the following cubic equation is obtained

$$\lambda_l^3 - 90A_1\lambda_l^2 + 1800\beta^2\lambda_l = 0, \quad (\text{A.1})$$

whose solutions are

$$\chi_1 = 0, \quad \chi_2 = 15 \left(3A_1 + \sqrt{9A_1^2 - 8\beta^2} \right), \quad \chi_3 = 15 \left(3A_1 - \sqrt{9A_1^2 - 8\beta^2} \right). \quad (\text{A.2})$$

Using the definition of the parameters A_1 and β , and after algebraic manipulations, it can be shown that the condition $9A_1^2 - 8\beta^2 > 0$ is equivalent to

$$\begin{aligned} & \frac{(\gamma_i + \gamma_{i,1})^2}{\eta_i\eta_{i,2}} + \frac{(\gamma_i + \gamma_{i,2})^2}{\eta_i\eta_{i,1}} + \frac{(3\gamma_i + \gamma_{i,1})^2}{5\eta_{i,2}^2} + \frac{(3\gamma_i + \gamma_{i,2})^2}{5\eta_{i,1}^2} + \frac{8\gamma_i^2}{5\eta_{i,1}\eta_{i,2}} \\ & + \frac{5}{4\eta_i^2} \left((2\gamma_i + \gamma_{i,1})^2 + 4\gamma_i\gamma_{i,2} + 2\gamma_{i,1}\gamma_{i,2} + \gamma_{i,2}^2 \right) > 0 \end{aligned} \quad (\text{A.3})$$

549 which is clearly satisfied for any choice of the material parameters. Therefore,
 550 the three solutions in Equation (A.2) are always real. More importantly, the
 551 maximum of the three solutions is always attained by χ_2 , meaning that this is
 552 the only relevant solution for the stability of the Leap-Frog scheme.

553 *Appendix A.2. Solutions corresponding to $\omega^2 = 1$*

Introducing $\omega^2 = 1$ into the characteristic polynomial of Equation (62), the following cubic equation is obtained

$$\lambda_l^3 - 3\sigma_1(1)\lambda_l^2 + 6\sigma_2(1)\lambda_l - 2\sigma_3(1) = 0, \quad (\text{A.4})$$

and the three roots are

$$\chi_4 = \tau_1 + \tau_3 + \frac{\tau_2}{\tau_3}, \quad (\text{A.5})$$

$$\chi_5 = \tau_1 - \frac{1}{2} \left(\tau_3 + \frac{\tau_2}{\tau_3} \right) + \frac{\sqrt{3}}{2} \left(\tau_3 - \frac{\tau_2}{\tau_3} \right) I, \quad (\text{A.6})$$

$$\chi_6 = \tau_1 - \frac{1}{2} \left(\tau_3 + \frac{\tau_2}{\tau_3} \right) - \frac{\sqrt{3}}{2} \left(\tau_3 - \frac{\tau_2}{\tau_3} \right) I, \quad (\text{A.7})$$

554 where $\tau_i = \sigma_i(1)$ for $i = 1, 2, 3$.

555 From the definitions in Equations (48) and (49), it is clear that τ_1 and τ_2
556 are real, whereas τ_3 can be real or complex.

557 If τ_3 is real, then χ_4 is real and χ_5 and χ_6 are complex. In this case only χ_4
558 is relevant from the point of view of the stability of the Leap-Frog scheme.

If τ_3 is complex then it can be shown that $\tau_2 = |\tau_3|^2$ by using Equation (49).
This implies that χ_4 , χ_5 and χ_6 are real and they can be rewritten as

$$\chi_4 = \tau_1 + 2\Re\{\tau_3\}, \quad (\text{A.8})$$

$$\chi_5 = \tau_1 - \Re\{\tau_3\} - \sqrt{3}\Im\{\tau_3\}, \quad (\text{A.9})$$

$$\chi_6 = \tau_1 - \Re\{\tau_3\} + \sqrt{3}\Im\{\tau_3\}, \quad (\text{A.10})$$

559 It is possible to prove that χ_4 is always the maximum of the three roots and
560 therefore it is the only relevant from the point of view of the stability of the
561 Leap-Frog scheme. Using the polar representation of a complex number, τ_3 can
562 be written as $\tau_3 = \sqrt{\tau_2}[\cos(\theta) + i\sin(\theta)]^{1/3}$ where $\tan(\theta) = \sqrt{\tau_2^3 - \tau^2}/\tau$. It is
563 worth noting that $\tau_2^3 - \tau^2 > 0$ because of the assumption of τ_3 being complex.

The application of the De Moivre's theorem [18] leads to

$$\Re\{\tau_3\} = \sqrt{\tau_2} \cos(\theta/3), \quad \Im\{\tau_3\} = \sqrt{\tau_2} \sin(\theta/3). \quad (\text{A.11})$$

564 Finally, it can be observed that, if $\theta \in [0, \pi)$, then $\Im\{\tau_3\} > 0$. This clearly
565 implies that $\chi_6 > \chi_5$. More importantly, $\theta \in [0, \pi)$ leads to $3\Re\{\tau_3\} > \sqrt{3}\Im\{\tau_3\}$,
566 which is equivalent to $\chi_4 > \chi_6$. An analogous argument can be used to prove
567 that $\chi_4 > \chi_5 > \chi_6$ when $\theta \in (-\pi, 0]$. It is worth mentioning that the case $\theta = \pi$
568 corresponds to τ_3 being real.

569 *Appendix A.3. Solutions corresponding to the roots of the polynomial T*

570 The number of real roots of the polynomial T depends upon the param-
 571 eters δ_1 and δ_2 . If $\delta_1 \neq 0$ the two roots of T are real, namely $-30(\delta_2 \pm$
 572 $\sqrt{\delta_2^2 - 2\beta^2\delta_1})/\delta_1$. If $\delta_1 = 0$ and $\delta_2 \neq 0$, there is only one real root, that is
 573 $-30\beta^2/\delta_2$. Finally, if $\delta_1 = \delta_2 = 0$, T has no real roots.

Introducing $\lambda_l = -30(\delta_2 \pm \sqrt{\delta_2^2 - 2\beta^2\delta_1})/\delta_1$ in Equation (62) leads to

$$\left(\delta_2 \pm \sqrt{\delta_2^2 - 2\beta^2\delta_1}\right)(2\delta_2 + 3A_1\delta_1) + 2\beta^2\delta_1(\delta_1 - 1) = 0, \quad (\text{A.12})$$

provided that $\delta_1 \neq 0$. Analogously, introducing $\lambda_l = -30\beta^2/\delta_2$ in Equation (62)
 leads to

$$\beta^2 + \delta_2(3A_1 + 2\delta_2) = 0, \quad (\text{A.13})$$

574 provided that $\delta_1 = 0$ and $\delta_2 \neq 0$.

575 From Equation (62), it is clear that the solutions corresponding to the roots
 576 of T correspond to the solutions described in Appendix A.1 (i.e. when $\omega = 0$)
 577 with extra restrictions on the material parameters given by Equations (A.12)
 578 and (A.13). Therefore, the solutions corresponding to the roots of the polyno-
 579 mial T are already included by the solutions given by Equation (A.2).

580 *Appendix A.4. Positivity of the solutions χ_2 and χ_4*

581 The positivity of the two solutions relevant to the stability of the Leap-Frog
 582 scheme, namely χ_2 and χ_4 , is discussed next. The positivity of χ_2 is clear as
 583 $\beta > 0$, $A_1 > 0$ and, as previously discussed, $9A_1^2 - 8\beta^2 > 0$.

In order to discuss the positivity of χ_4 , two cases are considered. If τ_3 is
 complex, it is possible to show that $\chi_4 = \tau_1 + 2\Re\{\tau_3\} > 0$ because $\tau_1 > 0$ and
 $\cos(\theta/3) > 0, \forall \theta \in (-\pi, \pi)$. It is worth noting that the condition $\tau_1 > 0$ is
 equivalent to

$$\frac{49\gamma_i}{5\eta_i} + \frac{\gamma_{i,1} + \gamma_{i,2}}{2\eta_i} + \frac{3\gamma_i + \gamma_{i,1}}{\eta_{i,2}} + \frac{3\gamma_i + \gamma_{i,2}}{\eta_{i,1}} > 0, \quad (\text{A.14})$$

584 which is clearly satisfied for any combination of the material parameters. Fi-
 585 nally, if τ_3 is real it is easy to show that $\tau_1 + \tau_3 + \frac{\tau_2}{\tau_3} > 0$ because it is the
 586 maximum root and the polynomial P of Equation (62) satisfies that $P(0) < 0$
 587 and $\lim_{\lambda_l \rightarrow \infty} P(\lambda_l) > 0$.